Research article

Initial nutrient condition determines the recovery speed of quiescent cells in fission yeast

Qi Liu [a,b], Nan Sheng [a], Zhiwen Zhang [c], Chenjun He [e], Yao Zhao [a], Haoyuan Sun [c], Jianguo Chen [a,b], Xiaojing Yang [a,*], Chao Tang [a,c,d,**]

[a] *Center for Quantitative Biology, Academy for Advanced Interdisciplinary Studies, Peking University, Beijing, 100871, China*
[b] *The Key Laboratory of Cell Proliferation and Differentiation of Ministry of Education, School of Life Sciences, Peking University, Beijing, 100871, China*
[c] *Peking-Tsinghua Center for Life Sciences, Academy for Advanced Interdisciplinary Studies, Peking University, Beijing, 100871, China*
[d] *School of Physics, Peking University, Beijing, 100871, China*
[e] *College of Life Science and Technology, Huazhong Agriculture University, Wuhan, 430070, China*

ARTICLE INFO

ABSTRACT

Most of microbe cells spend the majority of their times in quiescence due to unfavorable environmental conditions. The study of this dominant state is crucial for understanding the basic cell physiology. Retained recovery ability is a critical property of quiescent cells, which consists of two features: how long the cells can survive (the survivability) and how fast they can recover (the recovery activity). While the survivability has been extensively studied under the background of chronological aging, how the recovery activity depends on the quiescent time and what factors influence its dynamics have not been addressed quantitatively. In this work, we systematically quantified both the survivability and the recovery activity of long-lived quiescent fission yeast cells at the single cell level under various nutrient conditions. It provides the most profound evolutionary dynamics of quiescent cell regeneration ability described to date. We found that the single cell recovery time linearly increased with the starvation time before the survivability significantly declined. This linearity was robust under various nutrient conditions and the recovery speed was predetermined by the initial nutrient condition. Transcriptome profiling further revealed that quiescence states under different nutrient conditions evolve in a common trajectory but with different speed. Our results demonstrated that cellular quiescence has a continuous spectrum of depths and its physiology is greatly influenced by environmental conditions.

1. Introduction

Cellular quiescence is a reversible non-proliferating state, in which cell ceased growth and division but retained recovery ability to resume proliferation [1–3]. Endowed with this ability, quiescent cells function widely in many biological processes ranging from physiological, ecological, to pathological, e.g., tissue regeneration, seeds germination, plants longevity, chronic infection, and cancer relapse [4–9]. Functionally, this recovery ability can be dissected into two aspects, survivability and recovery activity, which depict

---

* Corresponding author.
** Corresponding author. Center for Quantitative Biology, Academy for Advanced Interdisciplinary Studies, Peking University, Beijing 100871, China.

E-mail addresses: xiaojing_yang@pku.edu.cn (X. Yang), tangc@pku.edu.cn (C. Tang).

how long a quiescent cell can survive and how fast it can recover, respectively. While the "how long" question has been extensively studied under the context of chronological ageing with stationary budding yeast cells [10–17] and fission yeast models [18–27], the "how fast" question has rarely been addressed quantitatively [28]. Although numerous factors, cellular components, and pathways that involved in the start, maintenance, and exit of quiescence states have been identified [1,26–35], how does the embedded recovery ability of quiescent cells evolve during persistent stresses and what factors influence this dynamics are still largely unknown.

There has been a long-standing debate about the nature of cellular quiescence [33,36,37]. It was thought to be an inactive dormant and distinct state, distinct from the cell cycle. This impression primarily derived from the observation that quiescent cells are typically arrested in G1 and exhibit a significant reduction in gene expression [18,38]. However, subsequent studies have revealed that cells can enter quiescence from phases of the cell cycle other than G1 [29,39]. Besides, both yeast and mammalian cells can access distinct quiescent states, each characterized by unique gene expression patterns, in response to various environmental signals [40–42]. Furthermore, both yeast and mammalian quiescent cells display diversity in quiescence depth and recovery activity [28,43]. All these
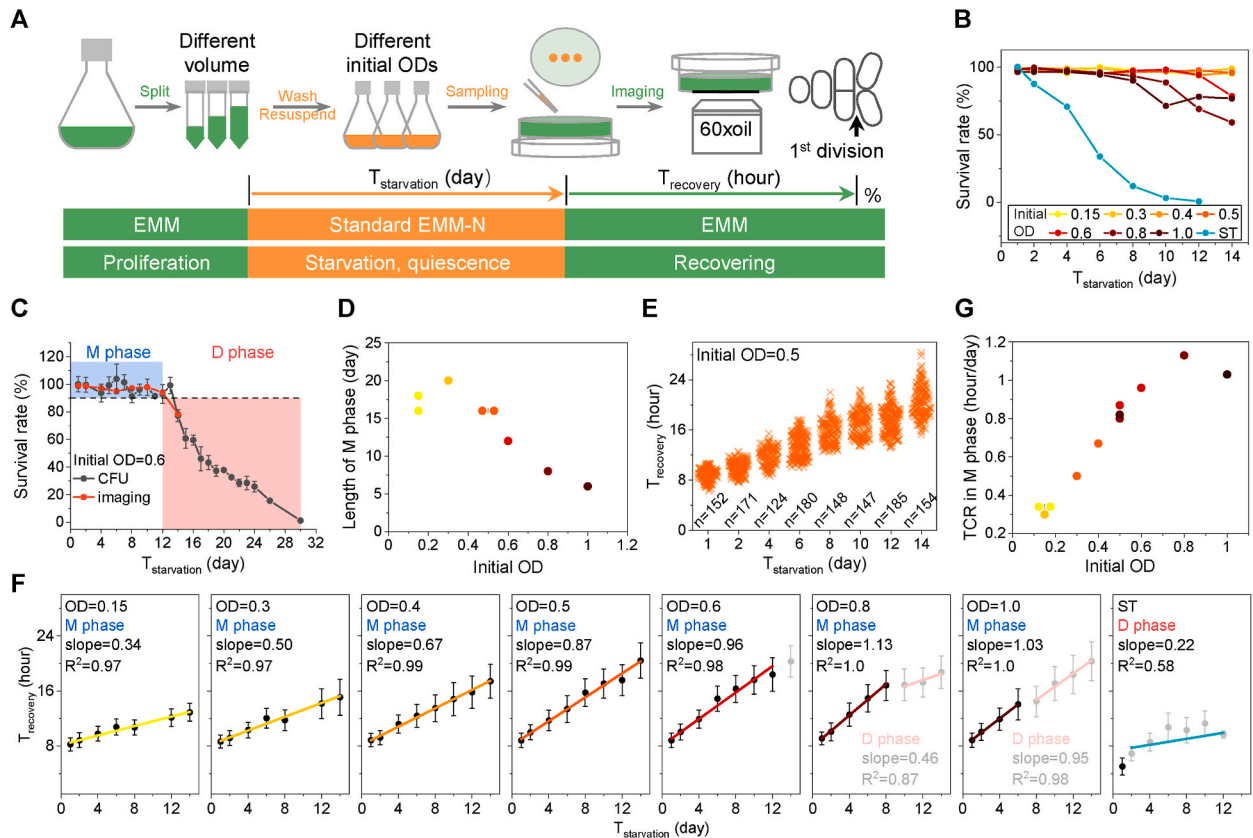
Fig. 1. Regenerative capability of quiescent cells under various initial OD conditions. **(A)** Schematic of experimental design for measuring single cell regenerative activity ($T_{recovery}$) of quiescent cells under different initial ODs. Different initial ODs were achieved by suspending different volumes of proliferating cells from the same growth culture into a fixed volume of standard nitrogen starvation medium EMM-N. Proliferating cells were washed three times with EMM-N-C prior to starvation. The same volume of growth culture was maintained as the ST control alongside nitrogen starvation treatments. The experiment was continued for two weeks and included 8 conditions, one of which was ST. The experiments were conducted in two batches with four conditions each, once. **(B)** Survival rate dynamics determined by imaging. Survival rate is defined as the percentage of cells that recovered. Detailed cell counts for total and recovered cells are provided in Table S1. More than 100 cells were analyzed for each sample. **(C)** The schematic description of M phase (survival rate≥90%, blue) and D phase (red) from survival rate curve measured by imaging (orange line), as exemplified by the condition of initial OD = 0.6. Survival rates measured by CFU counting (black line, data are means ± SEM and represented four repeats) are included for comparison. Both curves utilized identical sample sources. Analyses of all eight survival dynamics under different ODs are presented in Fig. S1A. **(D)** Correlation between the length of M phase and initial OD. The M phase length for the conditions of OD 0.5 and 0.15 in this experiment can't be obtained due to the longer survival time than experiment time, and their results were analyzed from the other two separated experiments containing the same condition (see Fig. 2C–S2A, S2B, and S4). The results for the condition OD = 0.3 was analyzed from the CFU data, see Fig. S1A. **(E)** Plot of $T_{recovery}$ against $T_{starvation}$ with initial OD = 0.5. Each cross represents a single cell and cell numbers are indicated. **(F)** Linear fitting of $T_{recovery}$ versus $T_{starvation}$ during the M phase. The results presented were derived from single experiments, with error bars for $T_{recovery}$ representing the standard error of the mean (SEM) from single-cell measurements. Linear fittings are indicated by the colored lines, while gray dots denote D phase data. Cell numbers are listed in Table S1. **(G)** The $T_{recovery}$ changing rate (TCR, defined as the linear fitting slope in **F**) under various initial ODs. The plot contains two additional repeats for ODs 0.5 and 0.15 derived from other two separated experiments (see Fig. 2C–S2A, S2B, and S4).

findings challenge the uniqueness and uniformity, instead highlighting the diversity and complexity of the quiescence state. Although the quiescence is now increasingly perceived as a dynamic and heterogeneous condition with varying depth, quantitative studies about how diverse the quiescence state could be and how deep it may reach are still lacking.

There are two models for quiescence study in yeast. The classical one is the carbon source exhaustion induced stationary phase (ST hereafter), which has been extensively studied in the budding yeast *Saccharomyces cerevisiae*. However, this model displays significant heterogeneity [44,45]. Besides, ST cells lost viability rapidly [46], thus are not suitable for studying the long-survived quiescence property. The other model is the nitrogen-starvation induced quiescence (Q_{-N} hereafter), which was mainly investigated in the fission yeast *Schizosaccharomyces pombe* [32].

The fission yeast *S. pombe* is a rod-shaped symmetrically dividing unicellular model organism for studying eukaryotic cellular biology and molecular biology [47]. Comparing with the asymmetrically dividing budding yeast *S. cerevisiae*, *S. pombe* shares more similarity with humans in gene structures, centromere complexity, homologous recombination, and RNA splicing [48]. Under nitrogen deprivation, rod-shaped proliferating fission yeast cells cease growth and reduce their size to smaller round-shaped and uncommitted G1 cells through two rounds of cell division within 6 h [18,32]. In the absence of the opposite mating type, these spherical cells enter quiescence state and can be easily distinguished from both the proliferating (long rod) and the stationary (short rod) cells [49]. Despite their quiescence, these cells remain metabolically active, are resistant to heat shock treatment, and exhibit dramatically different cytoplasmic and nuclear morphologies with a delayed cell cycle resumption in deep quiescence [18]. Comparing with the short-lived ST cells, Q_{-N} cells display greater morphologically uniformity and survival duration extending over several weeks and months [32]. These advantages make the fission yeast Q_{-N} quiescence an excellent model for investigating long-term quiescence and cellular aging. During the past two decades, the fission yeast Q_{-N} quiescence model has been developed into a complementary model beyond the yeast ST model, facilitating the study of both cellular quiescence and chronological aging [19,20,30,38,50–53].

To date, a significant number of quiescence-related studies have primarily focused on the identification of participating genes, regulatory mechanisms, metabolic changes, and organelle structural alterations during cell state transitions and quiescence maintenance. However, there has been a dearth of research specifically dedicated to the cellular recovery ability itself. In particular, the majority of studies have emphasized survivability or chronological lifespan, often overlooking the significance of cellular activity as another aspect of regenerative ability of quiescent cells. Hence, our research aims to quantitatively investigate the recovery ability of quiescent cells at the single cell level, focusing on their regeneration activity, with the hope of constructing a panoramic description of the yeast quiescence state landscape.

In this work, we used the Q_{-N} model and performed extensive and quantitative studies on the recovery ability of quiescent fission yeast cells at the single cell level. We traced the recovery behavior of up to 57,587 single cells under various nutrient conditions and starvation durations, and quantified their survivability and recovery activity. Additionally, we determined the depth of quiescence based on the single cell recovery activity. Together with time-course transcriptome studies, our large-scale, single-cell quantitative measurements enabled us to uncover the evolving dynamics of the quiescence state, the quiescence depth spectrum, and the factors that influence the regenerative activity of quiescent cells.

2. Results

2.1. Recovery time linearly increases with the starvation duration

To get a comprehensive view of how the recovery ability of wild-type quiescent fission yeast cells change with time and environment, we conducted nitrogen starvation with different initial conditions. Cells were plated on an agarose pad, and their recovery behavior as quiescent cells were monitored through time-lapse imaging microscopy (Fig. 1A). We quantified survivability and recovery activity at the single-cell level, measuring the survival rate and the recovery time, respectively. These parameters were derived from the time-course measurements. The recovery activity, specifically, was quantified by recovery time ($T_{recovery}$), counted from the time point quiescent cells re-engaged with growth medium EMM until the first cell division was completed (Fig. 1A). Note that shorter $T_{recovery}$ indicates higher recovery activity. The survival rate was calculated as the percentage of quiescent cells that successfully recovered and completed the first cell division. For detailed quantification see the Image analysis section in the Methods.

Given the inconsistency and lack of clarity in the quiescent cell concentration (indicated by optical density or OD) in existing literatures, it became necessary to provide a working frame to enable the comparison between different conditions. We first investigated the recovery ability of Q_{-N} cells with a wide range of initial ODs ranging from 0.15 to 1.0. The initial OD represents the suspension density of proliferating cells in the nitrogen-deprived medium EMM-N at the start of starvation. In practice, an initial OD was achieved by suspending an appropriate quantity of proliferating cells into a fixed volume of standard EMM-N (Fig. 1A, for details see the Quiescent cells preparation section in the Methods). The traditional ST condition was also included for comparison. The starvation and measurements with various initial ODs were carried out over two weeks.

Single cell quantification from the imaging data showed that the survivability of quiescent cells was declining with starvation duration ($T_{starvation}$) in an OD-dependent manner, cells with lower-OD survived longer (Fig. 1B–Table S1). After two-weeks' starvation, Q_{-N} cells still maintained full survivability under ODs below 0.5 while dropped visibly under ODs above 0.6 (Fig. 1B). Considering the quiescence state may be altered by the nutritional substances released from dead cells, we further divided the whole surviving dynamics into a maintaining phase (M phase, survival rate≥90%) and a decaying phase (D phase) (Fig. 1C). Note that, here, for simplification, the length of M phase did not exclude the initial entering phase (E phase) during which the cells reduce their size and shutdown the proliferation program [18,38]. The E phase lasts less than 6 h when judged by cell morphology [18], which is considerably shorter than the survival time. The length of M phase was negatively correlated with the cell density (Fig. 1D). The

survival rate measured by imaging showed a very good agreement with the measurements by traditional CFU (colony formation unit) counting (Fig. S1A, purple lines). Note that, unlike the Q_{-N} cells, the ST cells lost viability rapidly and the survival rate of ST cells started to drop since the very first day (Fig. 1B), which was consistent with previous studies [22,23]. This longevity of Q_{-N} cells enabled us to measure the single cell $T_{recovery}$ and trace its dynamics during long-term survival.

Single cell $T_{recovery}$ measurements showed that the recovery activity progressively declined with starvation duration ($T_{starvation}$) in all conditions including ST but with different speed (Fig. 1E–G, S1B and S1C). It was worth noting here that the overall $T_{recovery}$ of ST cells was significantly shorter than that of Q_{-N} cells (Fig. S1B), though its survival rate decreased rapidly, as mentioned above. This suggested a physiological distinction between ST and Q_{-N} quiescence.

Intriguingly, $T_{recovery}$ increased *linearly* with $T_{starvation}$ during the maintaining phase (M phase) under all conditions except for the ST case in which the M phase was too short to tell (Fig. 1F and S1E). The linearity was nearly perfect with the R^2 for linear regression being almost one (Fig. 1F). Here we define the linear fitting slope as the $T_{recovery}$ changing rate (TCR) for quiescent cells. We found that the TCR was positively correlated with cell density (Fig. 1G). However, there seemed to be an upper limit for both the M-phase length and the TCR under the standard EMM-N condition (Fig. 1D and G). Repeated experiments showed that the linear increasing behavior of $T_{recovery}$ was robust (Figs. S1C–S1E). We thus conclude that the recovery activity of quiescent cells decreases linearly with starvation duration before survivability decline and its speed is determined by the initial niche condition.

2.2. Excessive glucose impairs the recovery activity of quiescent cells

Our results, that lower OD led to higher recovery activity and that glucose-exhausted ST condition led to short survivability, indicate that the observed OD-dependent recovery activity may be due to the different nutrient availability for individual cells.
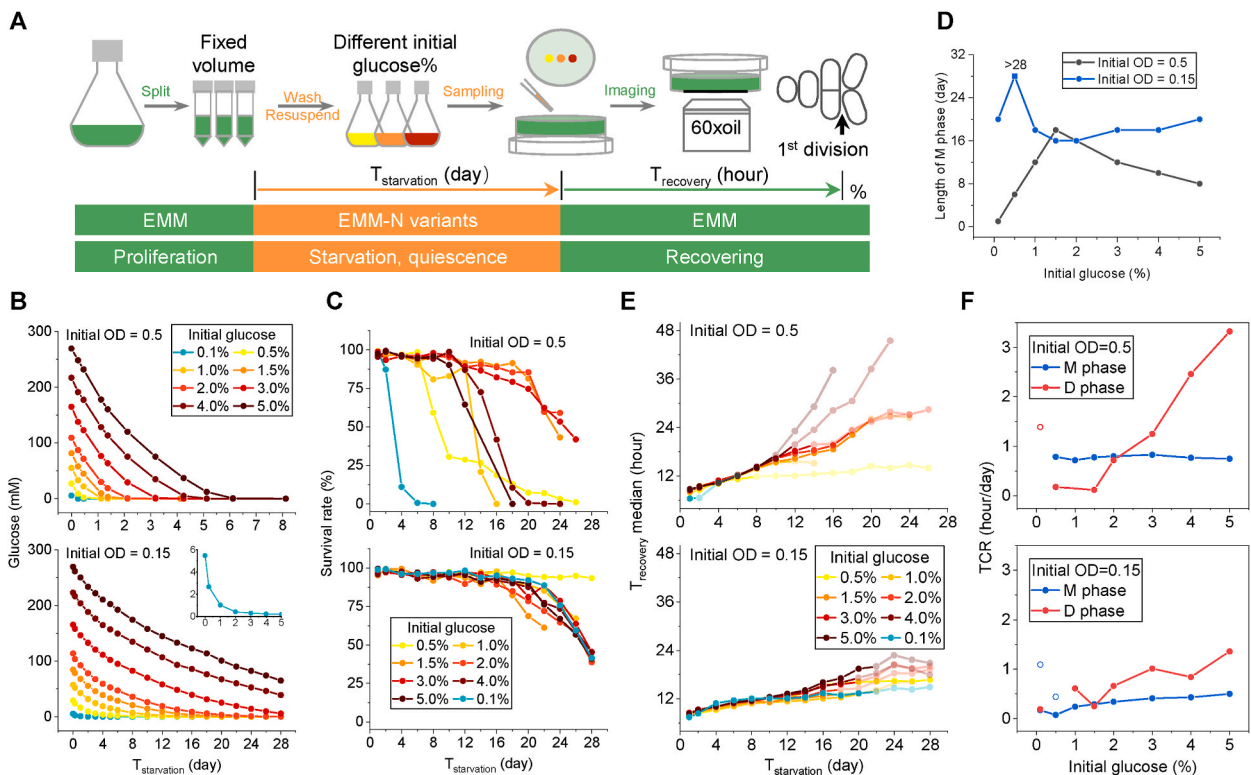
Fig. 2. Quiescent cell regenerative capability under various glucose conditions with two representative initial ODs. **(A)** Schematic of experimental design for measuring single cell $T_{recovery}$ of Q_{-N} cells starving with different initial glucose concentrations. This experiment follows the protocol of Fig. 1A with modifications of starvation media to vary glucose concentrations. EMM-N liquid variants with desired glucose concentration were employed. Proliferating cells were washed three times with EMM-N-C before resuspension in each media variant. The starvation experiment with the initial OD of 0.5 and 0.15 were performed separately in two separate batches, each comprising 8 different glucose conditions. The experiment lasted for one month and was performed one time. **(B–F)** Dynamics of medium glucose concentration (**B**), survival rate (**C**), length of M phase (**D**), single cell recovery time $T_{recovery}$ (**E**), and $T_{recovery}$ changing rate (TCR) (**F**). The data for $T_{recovery}$ in **E** were presented as medians, with the transparent portion indicating the decay phase (D phase). Mean ± SEM plots for $T_{recovery}$ are available in Fig. S2. Cell counts are provided in Table S2. TCR in **F** represents the slop of the linear fit applied to the $T_{recovery}$ dynamics, analyzed separately for the M and D phases. Detailed linear fitting results are shown in Fig. S3. The red circle in the up panel of **F** represents the TCR for rapidly dying Q_{-N} cells under the glucose deficient condition (initial 0.1% glucose with initial OD 0.5) as shown in Fig. S3A. Blue circles in the lower panel of **F** correspond to the TCR for the first part of M phase (M*) in Fig. S3B for two calorie-restricted conditions with initial OD 0.15.

Considering that glucose might be the most important nutrient during nitrogen starvation and that it has been reported to be a significant pro-ageing factor affecting the chronological lifespan of ST cells in both budding and fission yeast [14,22], we next investigated the recovering behavior of Q_{-N} cells under various glucose concentrations. We applied a wide range of initial glucose concentrations spanning from 0.1 to 5.0% under two representative initial ODs, 0.5 and 0.15.

To achieve different initial glucose condition, we made a series of EMM-N variants by substituting the 2% glucose in the standard EMM-N liquid medium with desired glucose concentration (Supplementary Table S7). Proliferating cells were washed three times with EMM-N-C before being resuspended into each EMM-N variant (Fig. 2A, for details see the Quiescent cells preparation section of the Methods). The initial glucose concentration corresponds to the glucose concentration at the start of starvation which is the same with the medium glucose level in each EMM-N variant. Meanwhile, we monitored the glucose level dynamics in the medium during nitrogen starvation. We found that the glucose consumption was significantly faster for the OD = 0.5 case than that of OD = 0.15 case. Glucose was exhausted within 7days under OD 0.5 but endured for more than 16 days (>0.2 mM) under OD 0.15 (except in the case of 0.1% initial glucose concentration) (Fig. 2B). This strongly suggested that quiescent cells are metabolically active and quiescence maintenance requires energy supply, consisting with the previous report by Yanagida group [18].

The survivability was influenced by the glucose availability in an OD dependent manner. We observed a much more significant change under different glucose concentrations for the OD = 0.5 cases (Fig. 2C–Table S2). We further quantified the length of the maintaining phase (M phase) for different cases. Interestingly, for both ODs, instead of a monotonic increase, we observed a bell-shaped change in M phase length with increasing glucose concentration (Fig. 2D–S2A and S2B). This indicated that, for a given cell density or initial OD, there exists an optimal glucose concentration for the survival of Q_{-N} cells, above which the glucose is detrimental. Moreover, different ODs showed different optimal glucose concentration. For our investigated glucose conditions, the optimal glucose concentration for OD = 0.15 was around 0.5%, which was much lower than the 1.5% for OD = 0.5 (Fig. 2D), suggesting again that cell density would affect the survivability of quiescent cells. We noted that, for initial OD of 0.15, the survivability was sustained, rather than significantly declined, at glucose concentrations above the optimal level, as indicated by the slight lifting in the M-phase length curve in Fig. 2D (blue line). This was due to the expansion of quiescent population under the relatively abundant nutrients supply created by the low cell density (as discussed later in Fig. 4F). The non-monotonic glucose effect on yeast survivability demonstrated that glucose also promotes chronological ageing under nitrogen starvation, similar to its effect under stationary condition which has been extensively studied.

For the recovery activity, $T_{recovery}$ increased linearly with $T_{starvation}$ before survivability decline in all cases with various glucose concentrations (Fig. 2E–S3A and S3B), which is consistent with previous results with different initial ODs (Fig. 1F). However, unexpectedly, during M phase with maintained survivability, while the $T_{recovery}$ increased significantly with the increase of OD under fixed nutrient condition (Fig. S3C), there was barely a change with the increase of glucose concentrations under fixed OD (Fig. S3D). Indeed, the $T_{recovery}$ under all glucose concentrations had not diverged until at the end of M phase (Fig. 2E, non-transparent part of the curves). Consistent with this, the $T_{recovery}$ changing rate (TCR) was almost the same in the M phase, especially for the OD = 0.5 case (Fig. 2F, blue lines). Thus, the effect of initial OD on recovery activity during M phase cannot be explained solely by glucose.

Interestingly, after entering the decaying phase (D phase), $T_{recovery}$ increased significantly with the increase of initial glucose concentration above the optimal point under both ODs (Fig. 2E, transparent part of the curves), suggesting that glucose exerted a profound influence on recovery activity mainly in the D phase. In addition, it is worth noting that, normally the TCR should decrease a bit in the D phase, since many substances were released into the environment after cell death, as we observed before (Fig. S1A, OD = 0.8 and 1.0). However, here as the system entered into the D phase, the TCR increased significantly with glucose concentration above the optimal concentration for both ODs (Fig. 2F, red lines), highlighting the strong detrimental effect of excessive glucose on the recovery activity in the D phase.

Note that we have included two calorie restriction (CR) conditions (0.1% and 0.5% initial glucose for OD 0.15 and 0.5, respectively) in our measurements. Though the effect of CR on chronological aging was widely investigated in various organisms, most of which focused on the life-span extension (survivability) and its mechanisms, little is known about the CR effect on the cellular activity of quiescent cells. In our nitrogen starvation system, we also observed the pro-longevity effect under the CR conditions in both ODs (Fig. 2C, bright yellow lines). The rapid loss of viability under OD 0.5 with 0.1% glucose was due to the glucose deficiency for individual cells under high cell density. Interestingly, although the survivability curve dropped early under OD 0.5 with 0.5% glucose (suggesting that the cells were also under the glucose deficiency condition to some extent), the curve leveled off later, implying that this CR condition had some effect on longevity. In addition, we found that Q_{-N} cells under CR conditions recover faster in D phase than that of under non-CR conditions (Fig. 2E).

Taken together, these results demonstrated that environmental glucose level is one significant influence factor both for the survivability and the recovery activity of quiescent cells.

### 2.3. The dependence of $T_{recovery}$ on OD is a combined effect of total nutrition

Since the effect of initial OD on $T_{recovery}$ cannot be explained solely by glucose as mentioned above, we then asked whether other nutrients take part in it. By simultaneously adjusting the concentrations of vitamin and mineral elements (VM hereafter) in the EMM-N medium (see Methods), we investigated the influence of non-glucose nutrients on the recovery ability of quiescent cells under two representative ODs (Fig. S4). Interestingly, increasing VM did not bring any significant effects but decreasing VM significantly impaired the survivability (Figs. S4A–S4C, Table S3). This suggests that long-term survival in quiescent state does not only require glucose but also other nutrients. For the recovery activity, increasing VM did not bring any positive or negative effect to the $T_{recovery}$, while decreasing VM influenced $T_{recovery}$ significantly, especially for OD = 0.5 case (Figs. S4D–S4F). Again, $T_{recovery}$ was linearly

increasing with $T_{starvation}$ for all VM cases studied (Figs. S4D and S4E). The $T_{recovery}$ changing rate (TCR) in M phase was unchanged under increased VM conditions but slowed down under decreased VM conditions (Fig. S4F, blue lines). These results suggested that deficiency in VM nutrients may contributed to the change in recovery ability. However, comparing with the significant effect of OD on $T_{recovery}$ in M phase, the effect of VM was rather limited. Thus, the effect of initial OD on $T_{recovery}$ cannot be simply explained by either glucose or VM. Given that most yeast quorum sensing systems primarily function in proliferating cells for either adaptive growth or development and require a threshold cell concentration [54], it is unlikely that the correlation between TCR and a wide range of OD in non-growing population is regulated by quorum sensing. Instead, the correlation is more likely due to the relationship between population density and single-cell nutrients availability. Taken together, we speculated that nutrients ratio and balance of glucose and other nutrients might be important, and the cell density dependence of recovery activity could be a combined effect of total nutrition.
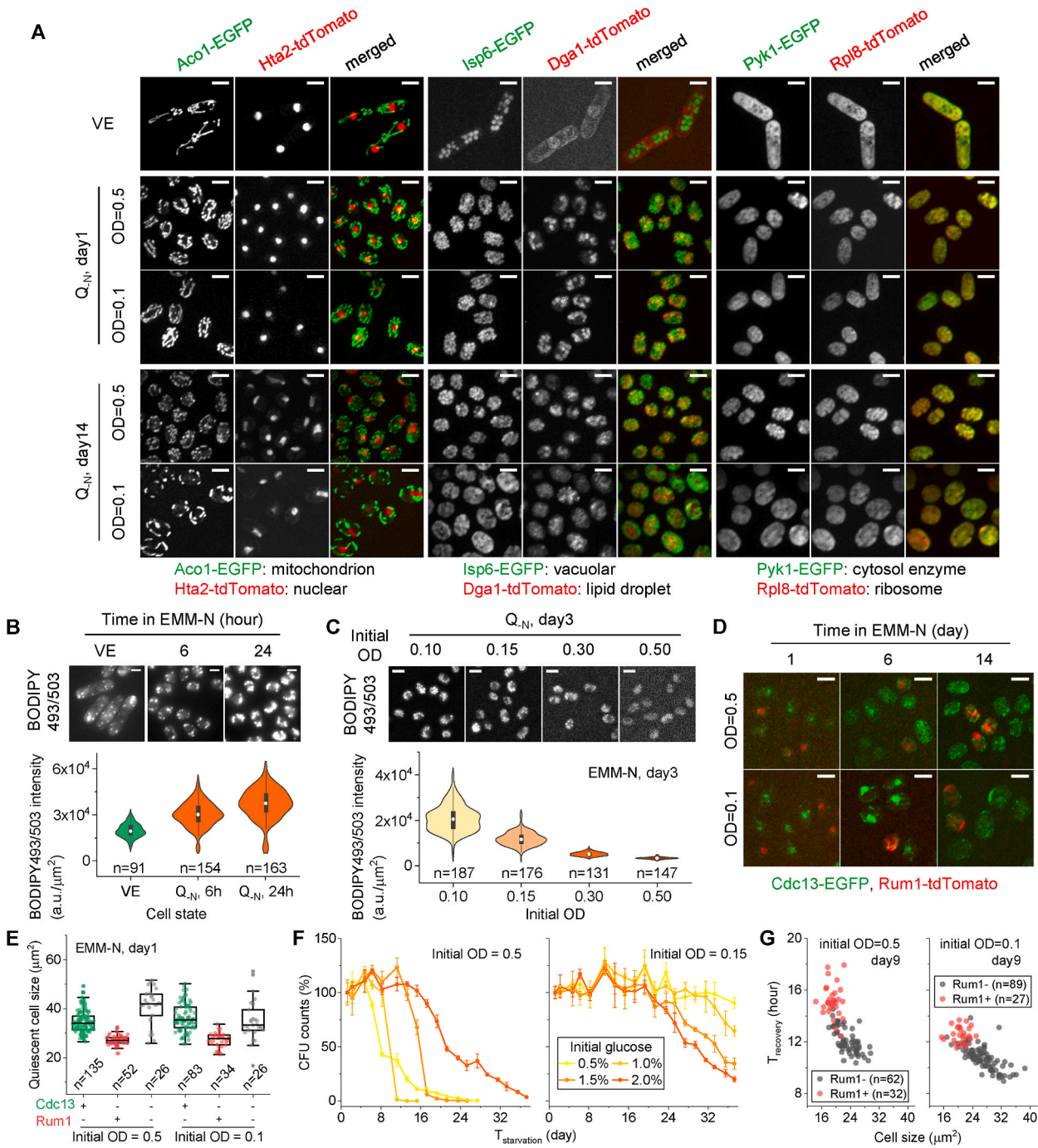
2.4. $T_{recovery}$ was negatively correlated with quiescent cell size

Although cell proliferation is ceased at quiescence state, we still observed cell size change under some conditions. Quiescent cell size was quantified as cell area (μm^2) from the starting image of the time-lapse imaging data by the software Cellseg developed by our group [55]. The quiescent cell size increased significantly under OD 0.15 but almost unchanged under OD 0.5, and slightly decreased under OD 1.0 (Fig. 3A and B, and S5A). The cell size change during quiescence state suggested again that quiescent cells are metabolically active, in agreement with the previous report [18]. It also supports the viewpoint that quiescent state is not static but evolving with time and environmental changes [37].

Cell volume has been reported to have strong influence on the speed of quiescence exit in budding yeast ST cells, with the larger mother cells recovering faster than smaller daughter cells [28]. To see whether this size effect on $T_{recovery}$ may also exist in the fission yeast Q_{-N} cells which are more homogeneous than ST cells, we then examined the correlation between $T_{recovery}$ and quiescent cell size. Indeed, we found the $T_{recovery}$ was negatively correlated with quiescent cell size under all conditions (Fig. 3C). Within the same population, larger quiescent cells recovered faster than smaller ones. To quantitatively investigate the influence of the quiescent cell size on $T_{recovery}$, we fitted $T_{recovery}$ vs. size data with linear regression and defined the absolute value of the fitting slope as "size sensitivity" (Fig. 3D), which quantifies how $T_{recovery}$ depends on quiescent cell size. For most ODs, the size sensitivity was progressively increasing with $T_{starvation}$, and $T_{recovery}$ was more depended on quiescent cell size at higher OD (Fig. 3E and S5B), suggesting the cellular reserve in quiescent cells is getting more important as the starvation duration increase especially for higher OD conditions. Interestingly, Q_{-N} cells under OD 0.15 seemed to maintain a constant size sensitivity (Fig. 3E and S5B), suggesting that they relied less on their own intracellular reserve, probably due to the relatively abundant niche resource under low cell density.
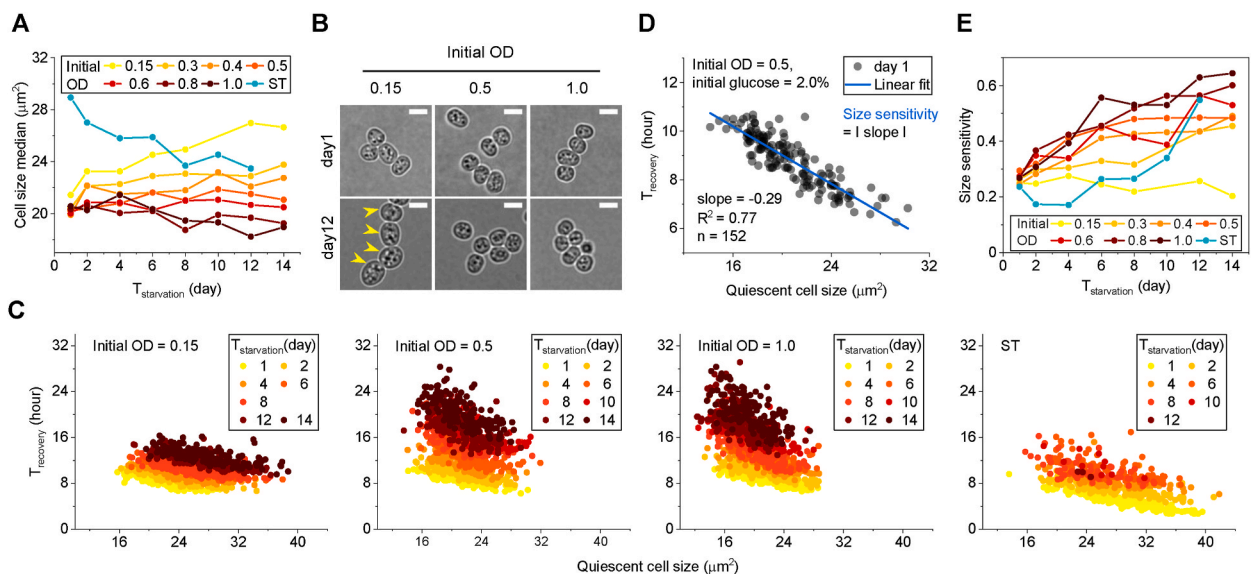
Fig. 3. Correlation between $T_{recovery}$ and quiescent cell size. **(A)** Comparison of quiescent cell size under various initial ODs. Median cell size is reported. Cell numbers are listed in Table S1. **(B)** Microscope images of typical Q_{-N} cells at day 1(up) and day 12 (bottom) under three initial ODs. Yellow arrows indicate the significant cell size swell or increase under the low cell density. The scale bar is 5 μm. **(C)** Inverse relationship between $T_{recovery}$ and quiescent cell size under all conditions, exemplified by the initial ODs of 0.15, 0.5, 1.0 and ST condition. Each dot represents a single cell. Cell numbers are listed in Table S1. **(D)** Linear fitting of the negative correlation between $T_{recovery}$ and quiescent cell size, exemplified by the initial OD of 0.5. The absolute value of the fitting slope is defined as "size sensitivity". Each dot represents a single cell. The linear fitting line is shown in blue, with the slope and associated metrics furnished. **(E)** Comparison of size sensitivity of ST and Q_{-N} cells across varying initial ODs. Note: Fig. 3A–E are associated with the findings presented Fig. 1.

A

Aco1-EGFP | Hta2-tdTomato | merged   Isp6-EGFP | Dga1-tdTomato | merged   Pyk1-EGFP | Rpl8-tdTomato | merged

VE

Q_{-N}, day1 OD=0.5 OD=0.1

Q_{-N}, day14 OD=0.5 OD=0.1

Aco1-EGFP: mitochondrion
Hta2-tdTomato: nuclear

Isp6-EGFP: vacuolar
Dga1-tdTomato: lipid droplet

Pyk1-EGFP: cytosol enzyme
Rpl8-tdTomato: ribosome

B Time in EMM-N (hour)

BODIPY 493/503   VE   6   24

BODIPY493/503 intensity (a.u./μm^2)

6×10^4, 3×10^4

n=91 n=154 n=163

VE Q_{-N}, 6h Q_{-N}, 24h

Cell state

C Initial OD Q_{-N}, day3
0.10 0.15 0.30 0.50

BODIPY 493/503

BODIPY493/503 intensity (a.u./μm^2)

4×10^4, 2×10^4

EMM-N, day3

n=187 n=176 n=131 n=147

0.10 0.15 0.30 0.50

Initial OD

D Time in EMM-N (day)
1 6 14

OD=0.5

OD=0.1

Cdc13-EGFP, Rum1-tdTomato

E EMM-N, day1

Quiescent cell size (μm^2)

60, 40, 20

n=135 n=52 n=26 n=83 n=34 n=26

Cdc13 + - - + - -
Rum1   - + - - + -

Initial OD = 0.5   Initial OD = 0.1

F

Initial OD = 0.5   Initial OD = 0.15

CFU counts (%)

150, 100, 50

Initial glucose
0.5% 1.0%
1.5% 2.0%

$T_{starvation}$ (day)
8 16 24 32

G

initial OD=0.5 day9   initial OD=0.1 day9

$T_{recovery}$ (hour)

20, 16, 12, 8

Rum1- (n=89)
Rum1+ (n=27)

Rum1- (n=62)
Rum1+ (n=32)

Cell size (μm^2)
16 24 32 40

(caption on next page)

Fig. 4. Global cellular remodeling in quiescent cells varies with initial OD. **(A)** Fluorescence microscope images of presentative functional proteins over different starvation durations under initial ODs of 0.5 and 0.1. Proteins are tagged with fluorescence markers and their representative functions are noted. **(B–C)** Comparison of lipids accumulation at various quiescence durations at an initial OD of 0.5 (**B**) and under various initial ODs at day 3 (**C**). The top and bottom panels in **B** and **C** display lipid visualization with BODIPY493/503 staining and quantification of lipid intensity in individual cells, respectively. Cells shown in **C** were washed by 1xPBS post-staining. **(D)** Fluorescence microscope images of cell cycle regulators at three quiescence time points for initial ODs of 0.5 and 0.1. **(E)** Size comparison of three quiescent cell (Q_{-N} cells) subpopulations exhibiting different cell cycle signals on day 1 under two initial ODs. Symbols "+" and "-" indicate presence or absence of nuclear located signals, respectively. The dim Cdc13-EGFP signal challenges clear discernment due to high background fluorescence, particularly at OD 0.5. Cells lacking clearly distinguishable nuclear signals are categorized as double "-". This group is a composite of cells, potentially including those with weak Cdc13 expression. **(F)** Survival rates of Q_{-N} cells under four glucose conditions at initial ODs of 0.5 (left) and 0.15 (right), determined via CFU counting. A comparison of quantified M phase duration with that measured by imaging is presented in Fig. S6C. **(G)** Comparison of $T_{recovery}$ of Q_{-N} cells with (Rum1+) or without (Rum1-) Rum1-tdTomato signal. Further comparison between roughly distinguished Cdc13 positive and negative cells within the "Rum1-" population is detailed in Fig. S6D. Each dot in E and G represents a single cell. The scale bar applies to all microscope images and is 5 μm.

2.5. Quiescent cells undergo global organelle and metabolic remodeling

Quiescence commitment typically involves remodeling of the intracellular structure and organization [18,31]. To get a better understanding of the evolutionary physiology of long-lived quiescence, we further monitored the changes of several intracellular components and key regulators during the starvation process, including mitochondrion, nucleus, vacuole, ribosome, cytosol, metabolic enzyme, lipid droplet, and cell cycle regulator. We labeled some key proteins with fluorescent tag and imaged their morphology and location at different starvation time-points under two representative initial ODs in standard EMM-N medium.

Comparing with vegetative proliferating cells (VE cells hereafter), Q_{-N} cells displayed obvious mitochondrion fragmentation (Aco1-EGFP), nucleus condensation (Hta2-tdtomato), vacuolar expansion (Isp6-EGFP), cytosol and ribosome granulation (Pyk1-EGFP and Rpl8-tdTomato), and lipid droplets accumulation (Dga1-tdTomato) under both ODs (Fig. 4A), suggesting a global organelle and metabolic remodeling during the quiescence development. Consistent with previous observation (Fig. 3B), we observed obvious increasement in quiescent cell size under lower OD, indicating by the cytosol proteins Pyk1-EGFP and Rpl8-tdTomato (Fig. 4A and S6A, day 14, OD = 0.1).

Mitochondrial dynamics is functionally adapted to cell bioenergetic requirements. High metabolic and respiratory activity promotes mitochondrial interconnection, whereas low energy demand leads to fragmentation [56]. After nitrogen deprivation, fission yeast cells under both ODs exhibited mitochondrial fragmentation at very early stage, one day after nitrogen deprivation (Fig. 4A, Aco1-EGFP). This occurred when medium glucose was still available (Fig. 2B), indicating a low energy demand for Q_{-N} cells. However, the fragmentation extent of mitochondria under two OD conditions was significantly different at deep quiescence. After two weeks of nitrogen starvation, mitochondrion appeared more fragmented compared to the day1 morphology for OD 0.5 case (Fig. 4A), indicating further decreased energy level and demand. Moreover, comparing with the OD 0.5 case, mitochondria in the OD 0.1 case at day14 exhibited less fragmentation and contained filamentous mitochondria (Fig. 4A), suggesting relatively high metabolic and respiratory activity under low cell concentration. Furthermore, the mitochondrion number seemed to have decreased under OD 0.1 at day14 comparing with at day1 (Fig. 4A), implying non-negligible mitophage events.

The condensation property of nuclear proteins significantly correlates with gene expression activity, high activity associates with liquid-like condensates whereas low activity with solid-like condensates [57]. Consisting with previous study [18], we also observed the nuclear condensation at deep quiescence state. The nucleus appeared flat and positioned at the edge of the quiescent cell after two weeks of starvation (Fig. 4A, Hta2-tdtomato), suggesting decrease in gene expression activity in long-starved quiescent cells.

Vacuole is an acidic organelle with degradation and storage functions [58]. The vacuole protease Isp6p in fission yeast was reported to be specifically induced by nitrogen starvation and participated in autophagy, which functions in nitrogen recycling by bulk degradation of intracellular proteins [59–62]. We found the number of vacuoles was significantly increased at the very early quiescence (day1, Fig. 4A), and their size was also enlarged as the starvation duration increased, especially for the lower OD case (day14, Fig. 4A), suggesting higher bulk degradation and nutrient storage capability during the quiescence development especially under lower OD. It is worth mentioning that, in both ODs, the cytosol glycolytic enzyme Pyk1-EGFP and ribosome protein Rpl8-tdTomato, which are both spreading in the VE cytosol, also displayed vacuole-like structures (Fig. 4A). Indeed, both Pyk1-EGFP and Rpl8-tdTomato were well co-localized with Isp6-containing vacuoles (Fig. S6A), suggesting the delivering of cytosol enzymes and ribosomes into the bulk degradation and nitrogen recycling system.

Lipid droplets (LDs) are the storage organelle of neutral lipids such as triacylglycerols (TAG) and play central role in lipid and energy homeostasis [63]. Fission yeast Dga1 is a triacylglycerols synthase and its deletion was reported to cause TAG deficiency and apoptosis in ST cells [64]. While in VE cells Dga1-tdTomato predominantly located in the nucleus and on the peripheral membrane, in Q_{-N} cells it was significantly up-regulated and largely located on LD membrane (Fig. 4A), suggesting increased triacylglycerols synthesis. LD-staining by BODIPY493/503 [65] confirmed the accumulation of lipids as cell entered into quiescence (Fig. 4B–Movie S1). Furthermore, we found quiescent cells accumulated more lipids under lower ODs (Fig. 4C). It should be noted that fission yeast cells form a basal level of LDs at proliferating state (Movie S2). However, these basal level lipids in LDs were quickly consumed in ST cells (Fig. S6B).

Supplementary data related to this article can be found online at https://doi.org/10.1016/j.heliyon.2024.e26558

Fission yeast cell cycle was driven by a major cyclin Cdc13 [66–68]. Cell cycle was blocked before G1 under poor nutrition by a negative regulator Rum1 [69], the expression of which is regulated by the nutrient-linked mRNA stability [70]. Before committing to a

state of quiescence, fission yeast cells experience two rounds of cell division that lack growth [18]. Interestingly, after quiescence commitment, the nuclear-located Cdc13-EGFP signal can still be seen in most cells, and only a small subgroup of Q_{-N} cells displayed Rum1-tdTomato signal (day1, Fig. 4D and E). In addition, Cdc13-EGFP signal mainly existed in bigger Q_{-N} cells while Rum1-tdTomato signal was exclusively expressed in smaller ones (Fig. 4E). After six days' nitrogen starvation, the nuclear-located Cdc13-EGFP signal was weakened under OD 0.5 but still sustained under OD 0.1 (Fig. 4D), suggesting Q_{-N} cells under lower cell density retained longer cell division activity. Consistent with this, CFU counting experiments showed that the quiescent population was obviously expanded under lower cell density condition, as evidenced by the longer maintaining phase measured by CFU compared to imaging (Fig. 4F and S6C). This suggested that some quiescent cells performed further cell division during the later quiescence stage. However, further into the nitrogen starvation, the Cdc13-EGFP signal was either disappeared or compacted into the condensed nucleus under both ODs (day14, Fig. 4D), suggesting the cell cycle program was eventually inactivated at old age. Generally, Q_{-N} cells with positive Rum1-tdTomato signal recovered slower than Rum1-tdTomato negative cells (Fig. 4G). These data demonstrated that quiescent cells are not necessarily exited the cell cycle after quiescence commitment, consistent with the previous study that quiescence development is not driven by cell
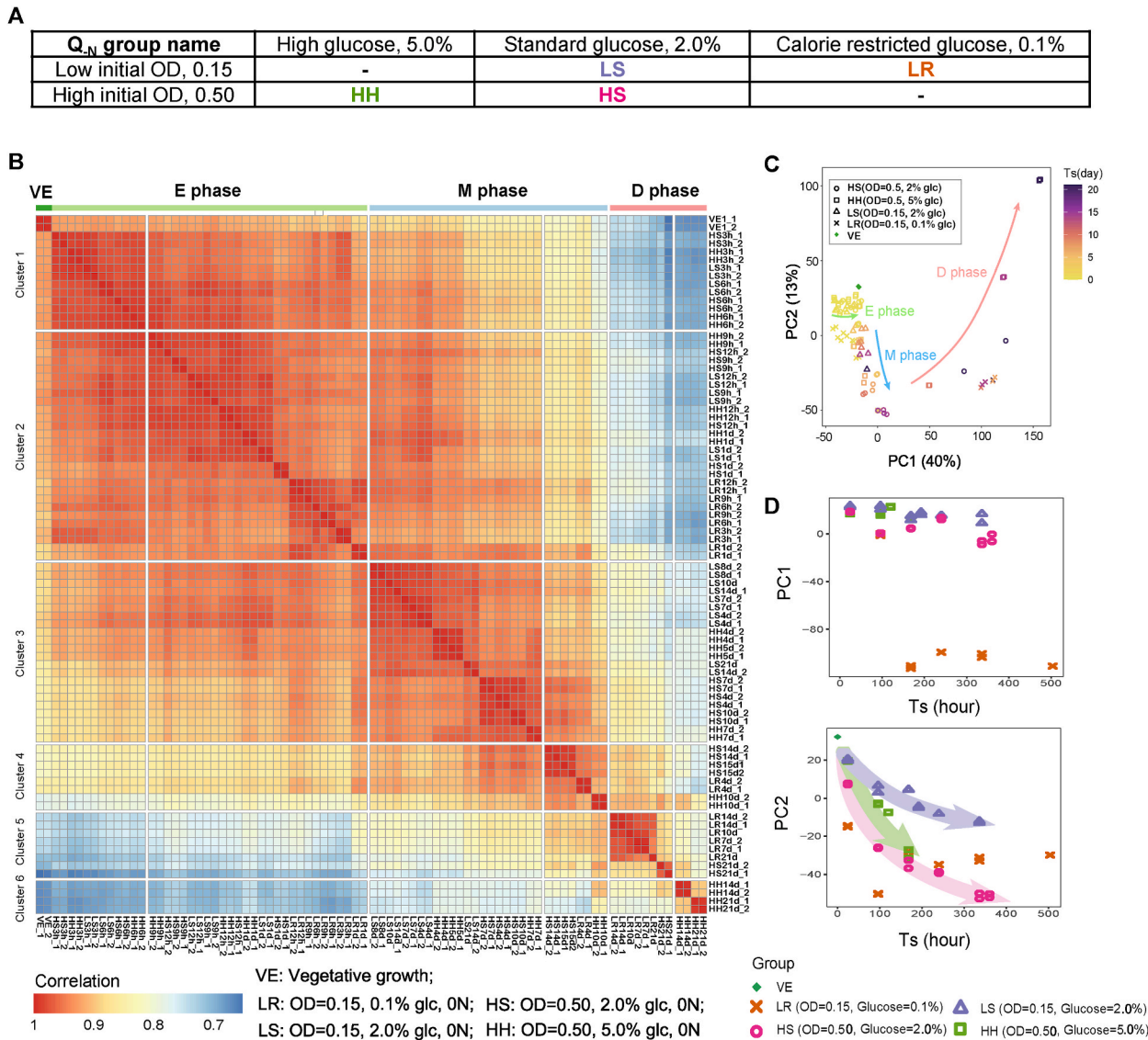
Fig. 5. Quiescent cells under various conditions follow a common ageing trajectory. **(A)** Detailed conditions for four different group of Q_{-N} cells. **(B)** Heatmap of correlation coefficients of overall gene expression between all samples. Color bar represents Pearson's correlation coefficient. Group conditions are indicated. **(C)** Principle Component Analysis (PCA) of the global gene expression pattern of all samples. Each dot represents a single sample. Color bar indicates starvation time (T_s). Shapes indicate different groups. Green, blue, and red guide lines indicate the general ageing trajectories during E, M, and D phase, respectively. **(D)** Projection of samples in in the M phase onto the first and second principal components(PC1 and PC2) as a function of starvation time T_s.
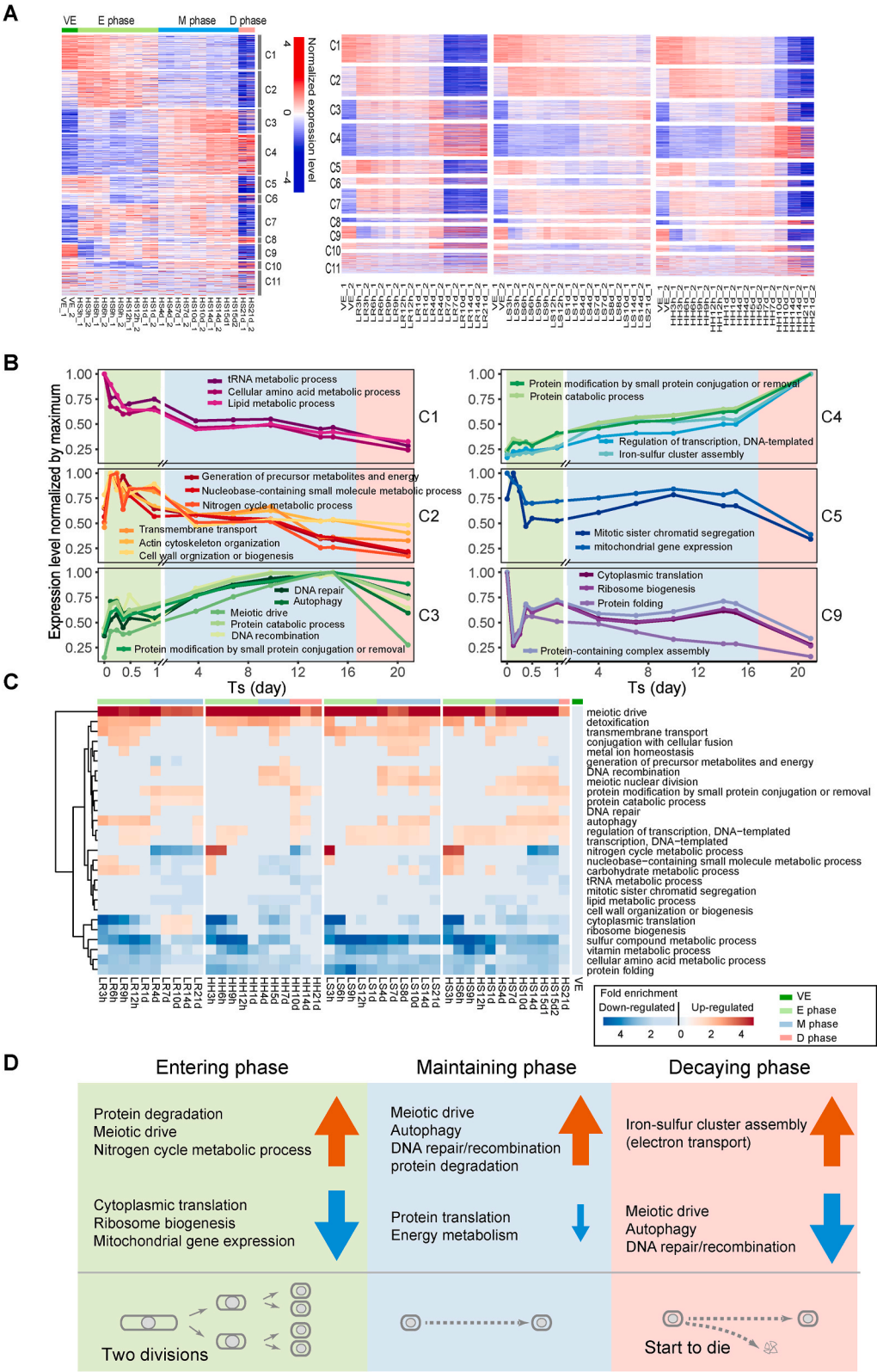
(caption on next page)

Fig. 6. Dynamic gene expression along the ageing trajectory. **(A)** Gene expression profile during quiescence development and cellular ageing under four group conditions. Color indicates the normalized gene expression level. Up- and down-regulations were shown in red and blue respectively. Sample names with time were shown on the bottom, developmental and ageing stage were shown on the top. Genes were clustered to 11 clusters by hierarchical clustering as shown on the right. **(B)** Expression dynamics of enriched gene functional modules within clusters identified in **A**n under the HS group condition. **(C)** Heatmap representing significantly enriched GO slim terms (rows) under four group conditions (columns) at different quiescence state compared with proliferating state (VE). Color bar indicates the fold enrichment of GO categories. **(D)** Overview of the gene expression changes characterizing quiescence development and ageing under nitrogen starvation.

cycle signals [29]. Depending on the cell density and quiescent cell size, quiescent cells may shut down the cell cycle program at different stages.

Taken together, these results suggested that the overall cellular organization and metabolism were remodeled during the quiescence development. However, the rate of remodeling varies among different components, and the extent of remodeling was greatly dependent on the environmental condition.

2.6. Quiescence states under different glucose conditions evolve in a common trajectory but with different speed

In order to explore the whole quiescence evolutionary dynamics during the nitrogen starvation at the molecular level, we further performed RNA-seq on Q_{-N} cells under four representative conditions (Fig. 5A) (group HS: OD = 0.5, 2% glucose; group HH: OD = 0.5, 5% glucose; group LS: OD = 0.15, 2% glucose; group LR: OD = 0.15, 0.1% glucose) at different time points (3hr, 6hr, 9hr, 12hr, 1d, 4d, 7d(8d), (10d), 14d, (15d), 21d). Note that group HS was taken as the standard condition for Q_{-N} cells and group LR for CR condition.

Here, we employed two distinct analytical approaches: Principal Component Analysis (PCA) and gene clustering. Both methods are commonly used in omics analyses, yet they serve different purposes. PCA, a dimensionality reduction technique, typically is used to lower the complexity of dataset and to identify key factors contributing to data variation, while gene clustering typically is used to group genes with similar expression patterns. We first put all the samples together and calculated the correlation coefficients of overall gene expression between all pairs. They clustered into six clusters (Fig. 5B). Interestingly, the six clusters turned out to be highly correlated with starvation time. The first and second clusters included all first day samples for all cases. The third and fourth clusters corresponded to maintaining phase samples, and the fifth and sixth clusters corresponded to the decaying phase samples. The only exception is that the late maintaining phase samples under the CR condition were clustered into the fifth cluster (Fig. 5B, group LR 7d, 10d and 14d). These results indicated that the quiescence processes under non-CR conditions may follow a similar trajectory. We further performed the principal component analysis (PCA) with all samples, and the result confirmed that non-CR conditions followed the same trajectory but with different evolving speed (Fig. 5C and D). Consistent with the previous finding that TCR increases with initial cell density (Fig. 1G), higher OD indeed had a higher evolving speed along the "quiescence trajectory" in terms of the global gene expression (Fig. 5D: PC2 group HS (rose red) vs. group LS (blue)), while no significant difference on evolving speed was found with different glucose concentrations (Fig. 5D: PC2 group HS (rose red) vs. group HH (green)).

2.7. Dynamic gene expression along the quiescence trajectory

Since all results indicated the existence of a common characteristic quiescence trajectory, we next investigated the gene expression changing pattern along this trajectory. The sequential change along the trajectory was reflected in 11 gene clusters that exhibited different temporal dynamic patterns (Fig. 6A). It is worth noting that after clustering, gene expression was found to be divided into four distinct stages along the quiescence development: VE state, entering phase (E phase), M phase and D phase (Figs. 5B and 6A), suggesting again the characteristic gene expression in different cellular states and quiescence stages.

We further did the functional enrichment within the 11 clusters, and found different expression dynamics for different functional modules (Fig. 6B and C). Take the group HS for example (Fig. 6B), after 24 h' nitrogen depletion, while the protein degradation and the nitrogen cycle metabolic process were upregulated, the protein translation and energy metabolism were downregulated dramatically. Meanwhile, meiosis related genes were also upregulated. As cells entered into the M phase, besides the further reduction of the protein translation and energy metabolism, meiosis related pathway kept being upregulated, and as well as the autophagy and DNA repair and recombination related genes (Fig. 6B). Then, in the D phase, the meiosis, DNA repair, DNA recombination, and autophagy related genes were all downregulated, and the electron transport related genes were upregulated. The characteristic quiescence development program for Q_{-N} cells was summarized in Fig. 6D.

We also looked into the difference between different glucose and OD conditions (Fig. 6C). As for the glucose concentration, though the evolving speed of the groups HS and HH were similar during the M phase, we still found some difference between them. Compared to 2% glucose, the detoxification related genes were significantly upregulated during the whole E-M-D process in 5% glucose. On the other hand, the upregulation of autophagy related gene can be detected during the whole M and D phases in 2% glucose, while it can only be detected at two time points in D phase in 5% glucose. These results suggested pro-ageing effect again for higher glucose concentration. As for the OD conditions, compared to OD = 0.5, we observed a significant higher level of transmembrane transport, cytoplasmic translation and ribosome biogenesis in OD = 0.15 (Fig. 6C), suggesting a higher energy state level and higher metabolic activity for the lower OD case.

It is worth noting that the CR case (group LR) was significantly different from the other three cases (Fig. 6C), which can also be seen on the PCA analysis (Fig. 5C and D). Firstly, no obvious upregulation of nitrogen cycle metabolic process related genes was seen. Secondly, autophagy related genes were upregulated at the very beginning of the starvation, while for non-CR conditions the

upregulation of autophagy was much later. Thirdly and most importantly, in the CR case the cytoplasmic translation and ribosome biogenesis were significantly upregulated in the M phase after day 7, which were even higher than that of VE state.

2.8. Quiescence state landscape is shaped by time and niche condition

Our results showed that the recovery ability of quiescent cells, both Q_{-N} and ST, was progressively declining with the starvation time with different speed under different conditions (Figs. 1F and 2E), suggesting quiescent cells can evolve into a large variety of states with different regeneration capability. These data strongly supported the viewpoint that quiescence is not a static "sleeping beauty" state [33] but evolving with time and having different depth [31].

To quantify the quiescence diversity, we introduced a dimensionless parameter named "quiescence depth" (QD) which was defined as $T_{recovery}/T_{cycle}$. T_{cycle} was the cell cycle time for VE cells and measured to be 2.5h on agarose dish (Fig. 7A). For comparison, we also included VE cells for QD analysis, with the cell division time of a full cell cycle taken as their $T_{recovery}$. While the QD distribution for VE
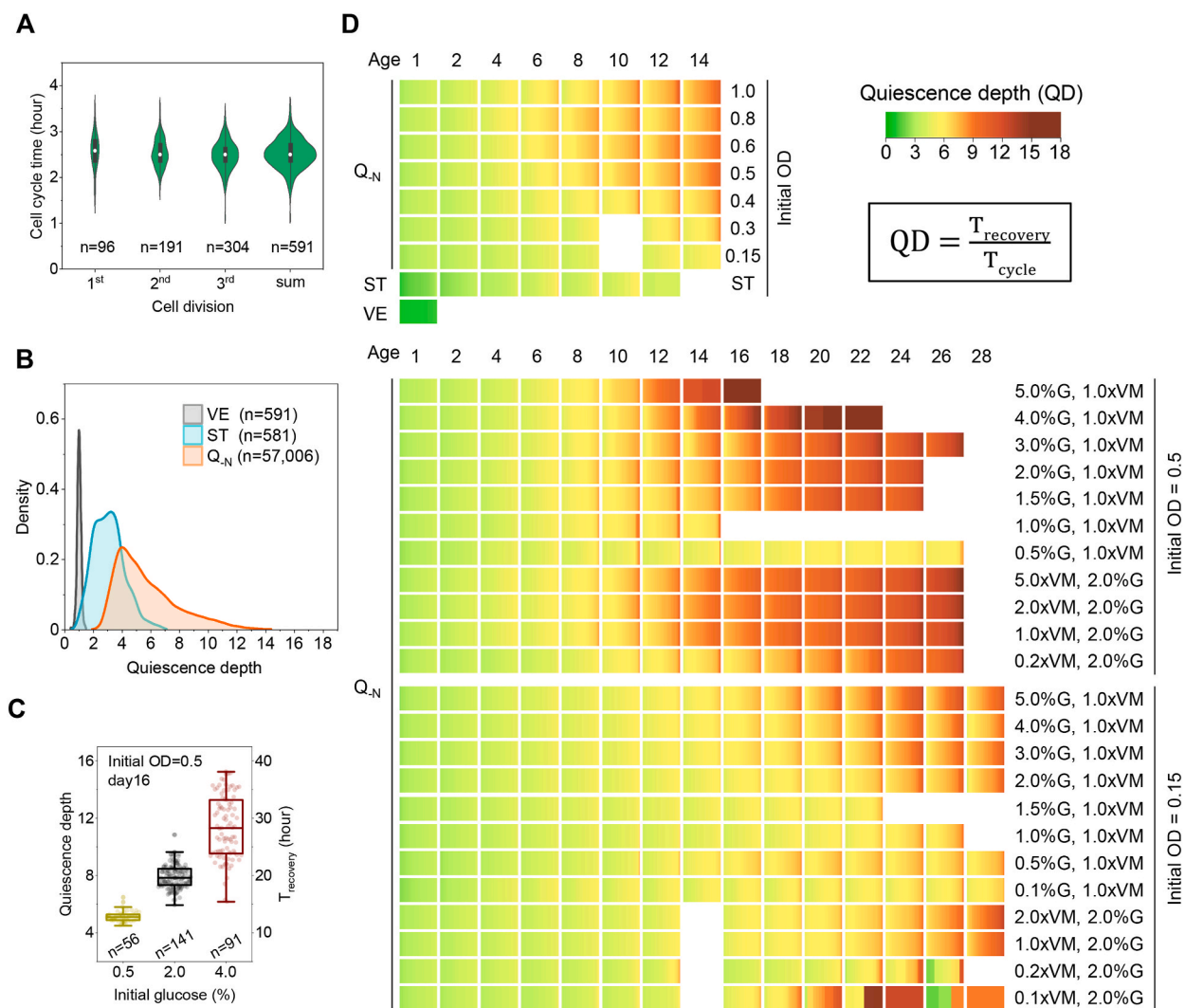
Fig. 7. Ageing quiescent cells can enter a large spectrum of states with various quiescence depth and regenerative capability. **(A)** Distribution of cell cycle time of proliferating fission yeast cells measured on agarose dish. Three sequential divisions with full cell cycle were analyzed. Cell numbers were indicated. **(B)** The quiescence depth (QD) distributions of VE, ST, and Q_{-N} cells. VE cell data corresponds to the aggregate "sum" from panel **A**. ST cell data aligns with the ST condition data in Fig. 1. Q_{-N} cell data amalgamates all Q_{-N} conditions from Fig. 1 and Fig. S4, with the total cell count for each category specified. **(C)** Comparison of QD of Q_{-N} cells at day 16 under three representative glucose conditions under the initial OD of 0.5. Boxplots illustrate data distribution and overlapped with single cell data points, each representing a single cell. The number of cells analyzed is indicated. **(D)** Comprehensive visualization of single cell QD across 32 niche conditions. Each block contains an array of colored strips representing single cell QD. Time points (ages) and specific conditions are indicated on the top and along the right side of each panel, respectively. Cell numbers are listed in Supplementary Tables S1–S3.

cells showed a narrow range with median value 1.0, the QD distributions for both Q_{-N} and ST cells were much wider (Fig. 7B). Interestingly, the QD distribution for ST cells showed a sizable overlap with VE cells, while there was no obvious overlap between the VE and Q_{-N} cells (Fig. 7B). It seems that the ST quiescence is an intermediate physiological state between proliferation and quiescence. Besides the wide range in QD distribution, Q_{-N} cells also displayed remarkable variation in QD (Fig. 7C). For example, for the OD = 0.5 cases, to fully resume proliferation after 16 days' nitrogen starvation, on average 5, 8, and 12 cycles' long time were needed for Q_{-N} cells under CR (0.5%), standard (2.0%), and high (4.0%) glucose conditions, respectively (Fig. 7C–Movies S3-S5). Particularly, under high glucose conditions, some Q_{-N} cells entered an extremely deep quiescent state, with $T_{recovery}$ extending to 48 h (Fig. 2E, OD = 0.5, 4.0% glucose, day22), significantly longer than the normal cell cycle time.

Supplementary data related to this article can be found online at https://doi.org/10.1016/j.heliyon.2024.e26558

The biological meaning for QD is that, the deeper the cell in quiescence state, the lower in recovery activity and slower in resuming proliferation. To get an overview of the quiescence state landscape for quiescent cells, we visualized all the single cell QD over various conditions (Fig. 7D). In total, we analyzed 57,587 single quiescent cells under 31 different niche conditions. All the QD constituted a beautiful continuous cell state spectrum (Fig. 7D). As shown by the spectrum constitution, the time and niche condition made up the two extrinsic dimensions for the quiescence spectrum. On one hand, the depth was gradually increasing with quiescence time or age. On the other hand, the recovery activity also greatly relied on the niche condition such as cell density and nutrient availability. In addition, the spectrum property also existed in the same population at any age, exhibiting quantitative heterogeneity underneath the qualitative homogeneity. During the maintaining phase, such as in early ages, the intrinsic variation in QD was relatively small (Fig. 7D). This heterogeneity was mainly generated from the cell size variation (Fig. 3C). However, after entered decaying phase, the QD heterogeneity was significantly amplified (Fig. 7D). This amplification was probably resulted from the changes in environmental nutrition caused by the release of intracellular contents from dead cells, suggesting that the extrinsic environmental influence on QD is larger than the influence of intrinsic cell size heterogeneity. Taken together, this wide spectrum of QD together with $T_{recovery}$ dynamics and survival curves illustrated that quiescence state is dynamic and plastic, and its landscape is shaped by time and niche condition.

3. Discussion

Survivability and recovery activity constitute the two key aspects of a quiescent cell's regenerative capability. While extensive efforts have been put into the studying on survivability, our study specifically focused on the recovery activity. Using the long-lived Q_{-N} quiescent fission yeast cells, we systematically quantified the recovery activity of quiescent cells at the single cell level. We monitored these dynamics under a wide range of nutrient conditions over month-long experimental periods. Our work provided the most profound evolutionary dynamics of quiescent cell regenerative capability to date. We found that fission yeast can enter a wide spectrum of quiescent states with significantly varied recovery activity ($T_{recovery}$). The $T_{recovery}$ is strongly influenced by the starvation duration ($T_{starvation}$), environmental condition, and quiescent cell size. During the evolution of quiescence state, the single cell $T_{recovery}$ was linearly increasing with $T_{starvation}$ before survivability decline and its changing rate (TCR) was predetermined by the initial niche condition.

Carbon source-exhaustion induced stationary quiescence (ST quiescence) is the prevalent yeast model in quiescence and aging studies. Much of our current understanding about cellular quiescence and chronological aging were contributed by the budding yeast ST model. Nevertheless, we found the Q_{-N} quiescence is significantly different from the ST quiescence in terms of cellular regeneration ability: Q_{-N} cells generally have higher survivability (longer M phase) but lower recovery activity (larger $T_{recovery}$) than ST cells (Fig. 1B and F). Furthermore, Q_{-N} cells accumulate substantial lipids, while ST cells are found in lipids exhaustion (Fig. 4B and S6B). Several other differences between these two quiescence models have been reported. For example, Q_{-N} cells mainly committed from G1 with 1C DNA content whereas ST cells predominantly arrested in G2 phase with 2C DNA content [18,32]. In addition, proteasome storage granules formation is observed in stationary phase but not under nitrogen starvation [71,72]. Moreover, a comparison of longevity genes screened from nitrogen starvation and stationary phase showed no overlap in gene orthologs [20]. These differences suggested that Q_{-N} and ST quiescence are two physiologically distinct quiescent states.

We propose that Q_{-N} and ST cells may adopt different strategies to better adapting to different nutrient stresses. It has been proposed that the natural environments of both fission and budding yeasts are rich in carbon sources but limiting in nitrogen sources [73,74]. Consequently, a deficiency in nitrogen is likely to persist for a long time, necessitating adequate preparation for a long-term survival. To this end, nuclear is condensed into a solid-like state for genome protection, many cellular components are degraded through autophagy for nitrogen recycling, and lipids are synthesized and stored in lipid droplets as a reserve of energy and nutrients. However, this strategic approach results in, as a cost, a reduced recovery activity and extended recovery time. This strategy can be supported by our previously demonstrated results in this work and reports by others [18,59,60]. On the other hand, despite the typically high availability of carbon source in natural environment, it not only serves as the main energy source, but also sustains a large number of competitors. Consequently, it might often run out momentarily but reappear soon after. Thus, ST cells need to respond rapidly to the incoming carbon source, rather than survive for a long time. To achieve this, functional organelles are primarily stored into storage bodies with remodeled structure and location, rather than being degraded after carbon source exhausted. This strategy can be supported by the remodeling of many organelles in stationary phase which were summarized in the review paper by Sagot and Laporte [31]. Considering the distinguished differences in recovery activity, survivability, and their dynamics between ST and Q_{-N} cells, it seems that the short-lived ST quiescence is specially developed for quick recovery under carbon-deficient but nitrogen-sufficient condition, while long-lived Q_{-N} quiescence is specifically developed for the long-term reservation of the regeneration potential under nitrogen-deficient condition. Since ammonium and glucose are two high quality nutrients, it would be interesting to know how the recovery ability of quiescent cells starved for other type of nitrogen and carbon source would evolve.

Glucose has been reported to be a pro-aging factor influencing the survivability of ST cells in both budding and fission yeast, that excessive glucose promotes aging whereas calorie restriction promotes longevity [14,22]. This glucose effect is also observed in Q$_{-N}$ cells (Fig. 2C and D). Interestingly, the recovery activity is also found to be influenced by glucose in a similar way, where high glucose impairs the recovery activity and low glucose improves it (Fig. 2E). It seems that the survivability decline is accompanied by the recovery activity loss. This leads to the question of whether the cellular survivability and recovery activity are coupled together or regulated by the same mechanism. This can be easily checked by examining the recovery activity of longevity mutants to see if they recover faster than the wild type.

It is worth mentioning that the impact of glucose on recovery activity only became apparent considerably later, after from the end of maintaining phase (Fig. 2E). This delay implies that, beyond the general quiescence deepening process, a threshold effect exists specifically resulting from excessive glucose and its metabolism. This consequence is so stronger that 48 h' long time is needed for some cells to manage it after nutrients refeeding (Fig. 2E). Considering the Q$_{-N}$ quiescence is physiologically distinct from the ST quiescence, it is worthwhile to figure out what glucose have done to quiescent cell at the molecular level, and whether this change is reversible during continued quiescence.

Remarkably, before quiescent cells start to die, the T$_{recovery}$ is linearly increasing with the T$_{starvation}$ in all cases (Figs. 1F and 2E, S1C and S4D). While it makes an intuitive sense that how fast a cell recovers from quiescence should depend on how long it had been in starvation, it was a real surprise for us to observe a nearly perfect linear relationship between T$_{recovery}$ and T$_{starvation}$ (R^2 almost equal to 1, Fig. 1F–S1E, S3A, S3B and S4E), especially considering that both starvation and recovery are complex processes involving dramatic changes in organelles morphology and global gene expression (Figs. 4–6). In order to get a sense how this may happen, we constructed a simple model and tried to interpret it in light of the experimental data. Assume that for our purpose the cellular state can be characterized by a single parameter, say some measure of the intracellular resource (R). Then during starvation cell consumes its intracellular resource R, say at a rate k_s, while during recovery cell replenishes this resource with a rate k_r until it reaches a threshold (R_{growth}) above which normal growth and division can resume (Fig. S7A). Mathematically,

$$R_{growth} = R_0 - \int_0^{T_s} k_s dt + \int_0^{T_r} k_r dt, \tag{1}$$

where R_0 is the value of the resource at the start of quiescence, and T_s and T_r are the starvation time and recovery time, respectively. It would be very difficult to have a linear relationship between T_r and T_s if the rates k_s and k_r were time dependent. On the other hand, if they are time independent, we have

$$R_{growth} = R_0 - k_s \bullet T_s + k_r \bullet T_r \tag{2}$$

or

$$T_r = \frac{k_s}{k_r} \bullet T_s + \frac{R_{growth} - R_0}{k_r}, \tag{3}$$

which relates T_r and T_s linearly with a slope k_s/k_r and an intercept $(R_{growth} - R_0)/k_r$. Our data (Fig. 1F and S1B) indicates that while the slope changes with OD, the intercept is the same for all cases (Fig. S7B), suggesting that the three parameters R_{growth}, R_0, and k_r are not dependent on the cell density of the starving population. This would further imply that the observed slope change in different cases of ODs (Fig. 1F) came from k_s: the higher the OD the larger k_s is. Thus, the experimentally revealed slope in Fig. 1F is a measure of k_s in our model, and the R in the model can also be regarded as a measure of recovery activity and quiescence depth. These results strongly suggest that the environmental niche condition at the onset of quiescence sets up the speed with which the quiescent state deepens, which in turn determines how long the cell needs to recover from quiescence.

Our work demonstrated that quiescence duration, environmental condition, and quiescent cell size are the three significant influencing factors to quiescent cell recovery activity. Among them, the quiescence duration and environmental condition are extrinsic while the size of the quiescent cell is an intrinsic factor. However, the impact of the quiescent cell size can also be affected by the former two factors (Fig. 3C and E). The influence of quiescence duration and quiescent size have been reported by previous study in budding yeast ST cells [28]. Here, we report that the initial niche condition prior to quiescence commitment is also a significant determinant of the quiescent cell recovery activity. Indeed, these initial niche condition not only influences the T$_{recovery}$, but also determines the T$_{recovery}$ changing speed (Figs. 1G and 2F). Together with time, they jointly shape the quiescence state landscape.

We have demonstrated that a quiescence state can evolve into an extremely deep state, requiring a substantial long time is needed for cell to resume proliferation. The variation in quiescence depth correlates with the different speed and extent of the global remodeling of cellular organelles and functional apparatus. Comparing with the parameter T$_{recovery}$, which measures the present cellular regeneration activity, its changing rate (TCR) could provide more information about the past environment condition and predict future outcomes. To this sense, TCR may reflect the chronological aging speed of quiescent cells. Taken together, our findings on T$_{recovery}$ dynamics, linearity, and the spectrum of quiescence depth gleaned from extensive single cell quantification provide a comprehensive view of the regeneration potential of quiescent cells, and may help to revisit the concept of cellular quiescence.

4. Materials and methods

4.1. Strains, plasmids, and media

All the fission yeast strains used in this study were congenic 972h- and listed in Supplementary Table S4. All fluorescence labeled genes were C-terminally tagged. Plasmids used for strain construction were listed in Supplementary Table S5. All constructs were confirmed by colony PCR. Oligonucleotides used in strain and plasmid construction were listed in Supplementary Table S6. Standard protocols were used throughout [75,76].

For construction of double-color strains LQF006, LQF068, LQF069, LQF072 and LQF079, plasmid PP004 and PP005 were used as template for the fluorescent cassette yEGFP-T$_{yADH1}$-kanMX6 and tdTomato-T$_{yADH1}$-natMX6 respectively. First genes were tagged with the fluorescent cassette yEGFP-T$_{yADH1}$-kanMX6 by two-step PCR [76] and the recombinant DNA were integrated into their endogenous locus. Successful transformants were selected by G418 (Sigma-Aldrich, Cat# A1720). Correctly integrated transformants were used for the second gene labeling. Second genes were tagged with the fluorescent cassette tdTomato-T$_{yADH1}$-natMX6 by the same method and integrated into their endogenous locus. The double-color constructions were selected with G418 and nourseothricin (GOLDBIO, Cat# N500). For construction of the strain LQF001, the first gene Cdc13 was tagged with yEGFP-T$_{yADH1}$-kanMX6 as previous. The second gene Rum1 was tagged with tdTomato and expressed under its native terminator T$_{Rum1}$. The recombinant DNA Left-leg$_{Rum1}$-tdTomato-T$_{RUM1}$-natMX6-Rightleg$_{Rum1}$ was first cloned into the plasmid PP008, then amplified by PCR from PP008 and integrated into the endogenous Rum1 site.

All plasmids were replicated in DH5α *Escherichia coli*. All constructs were confirmed by sequencing. The plasmid PP004 and PP005 were constructed by enzymatic digestion and ligation. Firstly, the kanMX6 cassette in the plasmid pDH3 was replaced with the natMX6 cassette from the plasmid pFA6a-natMX6 with *Bgl*II and *Eco*RI enzyme pair to generate the plasmid PP001. Then the CFP cassette in the plasmid pDH3 and PP001 were replaced by the yEGFP and tdTomato cassette from the plasmid PP002 and PP003 respectively with *Pac*I and *Asc*I enzyme pair. For construction of the plasmid PP008, the recombinant DNA Leftleg$_{Rum1}$-tdTomato-T$_{yADH1}$-natMX6-Rightleg$_{Rum1}$ was prepared by two-step PCR and then cloned into the T vector pMD19 to generate the plasmid PP006. Then the native terminator of Rum1 (T$_{Rum1}$) flanking with the *Asc*I and *Bgl*II cloning site was prepared by PCR and then cloned into T vector pMD19 to generate the plasmid PP007. At last, the terminator T$_{yADH1}$ in the plasmid PP006 was replaced by the T$_{Rum1}$ terminator from the plasmid PP007 with *Asc*I and *Bgl*II enzyme pair.

Synthetic media used for yeast culturing and quiescence maintaining are listed in Supplementary Table S7. All media were made according to the standard recipes [75]. All the liquid media were sterilized by 0.22 μm Millipore filters. YE agar plates with or without drug were used to select fluorescence constructions or grow CFU colonies respectively. Liquid EMM and EMM (EMM lacking NH4Cl) including EMM-N variants (EMM-N with different level of glucose or VM) were used to prepare proliferating and quiescent cells respectively. The EMM-N variant with different glucose or VM level was adjusted by simply replacing the 2% glucose in standard EMM-N medium with desired glucose concentration, or replacing the standard VM concentration with desired VM concentration. Each EMM-N variant has only one component adjusted, which is either glucose for Fig. 2 or VM for Fig. S4. The EMM-N-C (EMM lacking NH4Cl and glucose) liquid medium was used to wash proliferating cells before re-suspending into standard or variant EMM-N. EMM with 1.5% low melting temperature agarose (Lonza, Cat# 50080) was used for time-lapse imaging the recovery of quiescent cells. EMM agarose containing 1ug/ml BODIPY493/503 (Invitrogen, Cat# D3922) was used for imaging the dynamics of lipids droplets in proliferating cells. All media ingredients related to synthetic media were chosen as Sigma BioUltra grade to eliminate the possible nitrogen contamination caused by the nitrogen residue in each ingredient.

4.2. Microscope agarose dish preparation

Petri dish with a removable glass bottom (NEST Cat# 801002) was used to make EMM agarose dish. The original round glass bottom was removed and replaced by a square microscope cover glass (Fisher 12–542A) and sealed with Scotch tape (Cat# 810QC33). 20 ml EMM liquid medium containing 1.5% (m/v) low melting temperature agarose was microwaved for no more than total 45 s and then cooled down to below 37 °C under running water. For lipids droplets imaging, additional 20 μl 1 mg/ml BODIPY493/503 was add to the 20 ml cooled EMM agarose. 2.7 mL cooled liquid EMM agarose medium was immediately filled into the reconstructed Petri dish and then thoroughly solidified at room temperature for about 3 h. Before use, the agarose dish was inverted for 0.5 h for easily tearing off the square cover glass without damaging the smooth agarose surface. The agarose dishes were freshly made before use on the experimental day. Just before loading cells, tear off the cover glass and dry the surface for several seconds at room temperature. Then drop 0.1 μl cell suspension on the agarose surface and array all samples in the central region of the imaging area with a designed order. After each sample loaded, dry the sample spot for several seconds. Make sure all loaded spots are isolated and not cross diffused into each other. When all samples were settle down, record the time and then seal the agarose with a new clean cover glass and fix it with Scotch tape but leaving an imaging area as large as possible. It is essential to make sure that, (1) the agarose is thoroughly solidified, (2) the agarose surface is smooth after teared off the cover glass, (3) agarose surface is dried before loading each sample, otherwise the loaded cells will be cross diffused. After sophisticated, a ready-for-imaging microscope agarose dish loaded with up to 10 isolated samples can be made within 5 min.

4.3. Quiescent cells preparation and starvation under different initial conditions

A sufficient volume of proliferating culture was made first prior to starvation experiment. In brief, inoculate a single colony into 50

ml EMM liquid and grow to the OD600 around 1.0. Then inoculate 10 ml culture into several flasks of 300 ml EMM and grow to the OD600 of 0.5–1.0. Then mix all the 300 ml-culture together and measure the OD600 of the pooled culture, whose OD600 value was then used for calculating the volume of proliferating cells needed for preparing quiescence culture with the desired initial OD. In the same batch of starvation experiment, all the different initial conditions were made from the same pool of proliferating culture.

To make Q_{-N} cells with different initial OD (OD600 = 0.15, 0.3, 0.4, 0.5, 0.6, 0.8, 1.0) (Fig. 1), proper volumes of the pooled proliferating cells were harvested together by centrifugation and washed three times in EMM-N-C liquid. After wash, each pellet was re-suspended into 200 ml standard EMM-N liquid to accomplish the designed initial OD. 200 ml proliferating cells was split out from the pool and labeled as ST. Then all samples were taken into the same shaker and starved together.

To make Q_{-N} cells with different initial glucose (Fig. 2), aliquots of the pooled proliferating cells with fixed volume were harvested together by centrifugation and washed three times respectively in EMM-N-C liquid. Then each pellet was re-suspended into one EMM-N variant at a final volume of 200 ml. The glucose level of each EMM-N variant is the initial glucose level for Q_{-N} cells starved in it. The experiment for starving yeast with different initial VM (Fig. S4) was performed similarly as glucose but using another serious of EMM-N variants with different VM levels (Supplementary Table S7). All the EMM-N variants were made in advance and split out before culture manipulation in the experiment day.

The time when all the washes finished was recorded as the T0 for nitrogen starvation and shared by the ST condition. During continuous starvation, 1 ml culture was taken out at each indicated time-point and split into 3 parts, 200 μl for serial dilution for CFU plating, 200 μl for agarose dish sampling, remaining 600 μl for supernatant collection and glucose level measurement. The supernatant was stored at -20 °C before batch measuring. The sampling and measurements were continued for one month. All liquid yeast cultures were incubated at 30 °C with shaking (220 rpm).

4.4. Time-lapse imaging

Time-lapse images were acquired at 5 min interval with a Nikon Eclipse Ti Microscope equipped with an automated stage, a perfect-focus-system, an 60× oil immersion objective, an Evolve EMCCD camera, and built in NIS-Elements softerware. For measuring the cell cycle time, agarose dish loaded with proliferating cells were pre-cultured for 2 h on microscope at 30 °C and then imaged for 12 h. For measuring the $T_{recovery}$ of quiescent cells, time-lapse program was immediately started after imaging program settle down. Before time-lapse imaging, one loop capture was performed to verify the program works correctly and the lens oil disperses homogenously. This one-loop images were subjected for cell segmentation and cell size extraction with the CellSeg software [55]. Upon the start of the time-lapse imaging program, recorded the time as T0'. The imaging duration was set as 16 h at day1 and extended accordingly in the following days. During imaging, if cells were found off focus, the imaging program was paused to re-adjust the focus. The pause interval was automatically recoded by the program and taken into account for calculating the single cell recovery time. All microscope agarose dishes were maintained at 30 °C during imaging.

4.5. Yeast cells immobilization

Before fluorescence imaging, yeast cells were immobilized to the microscope plate which was coated with Concanavalin A (Sigma-Aldrich, Cat# C2010). For coating 384well microscope plate (Cellvis, Cat# P384-1.5H–N), fill each well with 20 μl Concanavalin A water solution (2 mg/ml) to cover the glass surface. After 2mins' coating, remove the solution and dry the plate for several hours. To immobilize yeast cells, drop 5 μl cell suspension into the coated well, then add 15 μl 1× PBS into the well to achieve a proper cell density. Centrifuge the plate for 30 s at 500g to sediment and immobilize yeast cells.

4.6. BODIPY493/503 staining

BODIPY493/503 (Invitrogen, Cat# D3922) was dissolved in DMSO at 1 mg/ml and then divided into 100 μl aliquots and stored at -20 °C under dark as 1000× stock. For lipids staining, add 1 μl 1 mg/ml BODIPY493/503 stock into 1 ml yeast suspension and stain for 10min under dark. After staining, load 5 μl of each stained sample into the wells of 384-well microscope plate which coated with Concanavalin A and then add 15 μl 1× PBS into each sample and mix well. Centrifuge the plate for 30 s at 500g to sediment and immobilize yeast cells. After immobilization, detect BODIPY493/503 fluorescence with a confocal microscope. If not specially mentioned, the stained samples were not washed by 1× PBS before loading into wells.

4.7. Confocal fluorescence microscope

To investigate the organelle morphology and target gene expression under quiescence state, double-color fluorescence strains were imaged with confocal fluorescence microscope. Images were taken with a 100× oil TIRF objective plus 1.5× intermediate magnification. During imaging, yeast cells were sliced for 15 layers within 4um thickness. More than 100 single cells were imaged for each sample.

4.8. CFU plating

Before plating, cultures were serially diluted to appropriate concentration (100–150 cells per 100 μl) by EMM liquid. The diluted concentrations for samples with different initial OD were 7.0×10^{-5}, 3.5×10^{-5}, 2.5×10^{-5}, 2.0×10^{-5}, 1.5×10^{-5}, 1.25×10^{-5}, 1.0

$\times\ 10^{-5}$, and 1.0×10^{-5} for initial OD of 0.15, 0.3, 0.4, 0.5, 0.6, 0.8, 1.0 and ST respectively. Then 200 µl end dilution was plated on to each YE agar plate with 4 repeats plated for each sample. After 3 days of incubation at 30 °C, the colonies on each plate were counted. The survival rate measured by CFU method was calculated as the percentage of colony counts at each time-point relative to the reference counts at day 1.

4.9. Glucose concentration measurement

The culture medium glucose concentration was measured by Glucose Oxidase Method with a commercial assay kit (Applygen Technologies, Cat# E1010). Samples were the −20 °C stocks of supernatant collected during each imaging experiment.

4.10. Image analysis and $T_{recovery}$ quantification

Time-lapse images were exported with NIS-elements software. Images were analyzed with the software "Cellseg" [55]. All cells in the analyzed image were segmented. Those edge cells which later moved out of the field during time-lapse imaging were excluded for statistical analysis. More than 100 single cells were analyzed for each imaged sample (cell number details see Supplementary Tables S1–S3).

For single cell recovery time ($T_{recovery}$) measurement, the single cell recovery behavior of quiescent cell was traced by eye and the image frame number "m" of first cell division was recorded by hand. The $T_{recovery}$ for each single cell was defined as the time duration starting from dropping cells on agarose dish until the first cell division finished. $T_{recovery}$ was the imaging time obtained from imaging data plus experimental time. Generally, $T_{recovery}$ (minute) $= 5(m-1) + T0'-T0$, with T0 and T0' are hand-recorded time during microscope agarose dish preparation and time-lapse imaging (see Time-lapse imaging). If there is a pause during imaging due to the re-tuning of the imaging focus, the pause time is taken into account. The survival rate measured by imaging was calculated as the percentage of fully recovered cells which finished first cell division in the analyzed population.

For fluorescence image analysis, all slices for each fluorescence channel were stacked into 1 Gy image by Z projection with maximum tensity with the software Fiji [77]. The Z-projected gray image of each channel was background-subtracted and then merged into one RGB image. The "substract background" function of Fiji was used and the rolling ball diameter was set as 30.

For cell size measurement, images were analysis with the software "Cellseg". All cells fully presented in the image filed were segmented. All imprecise segmentations were corrected by hand using the build-in function of "edit segmentation" of the software "Cellseg". The measurements of cell area and cellular fluorescence were exported by the "export" tool in the Cellseg.

4.11. cDNA library preparation and RNA-seq

RNA was isolated using TRIzol (Thermo Fisher Scientific, Waltham, MA, USA). mRNA molecules were purified using the poly-T oligo attached magnetic beads following which the mRNA was fragmented and primed for cDNA synthesis. cDNA libraries were pair-end 150-bp sequenced on the DNBseq platform at BGI (Wuhan, China).

4.12. RNA-seq data preprocessing

Raw sequences were filtered by SOAPnuke [78]. HISAT2 [79] was used to align the RNA sequencing reads to the Schizo-saccharomyces pombe reference genome (https://www.pombase.org/downloads/genome-datasets). Paired-end cleaned reads were mapped to the reference genome using Bowtie2 [80]. The number of mapped reads covering each gene and FPKM were calculated using RSEM [81].

4.13. RNA-seq data analysis

To study the similarities between all samples, we performed log2 transformation on the FPKM matrix and calculated the Pearson correlation coefficients between the two samples. The log2 transformed expression matrix was subjected to Principle Component Analysis to visualize the sequential transition of transcriptome.

For gene expression clustering analysis, FPKM was log2 transformed. The R package WGCNA [82] was used to detect clusters of highly correlated genes. Clustering results were visualized as heat maps using the R package pheatmap. The GO biological process slim table from the Pombe website (https://www.pombase.org/browse-curation/fission-yeast-bp-go-slim-terms) was used as an annotation for the genes. GO terms enriched in WGCNA clusters were detected using the function 'enricher' in the R package clusterProfiler [83]. The average expression levels of genes included in the GO terms with Holm-Bonferroni-corrected p-value <0.05 were shown in Fig. 6B.

To globally visualize the functional modules regulated differently under different cell densities and glucose concentrations during the quiescence development, the functional enrichment of all samples relative to proliferative state samples was shown in Fig. 6C. For this analysis, differentially expressed genes between all samples and proliferative state samples were detected using the R package DESeq2 [84]. The cut-off for significance was the adjusted p-value <0.05 and the fold difference >2. This analysis generated a list of significantly up and down-regulated genes for each group. These gene lists were analyzed using the function 'enricher' in the R package clusterProfiler. GO slims with a Holm-Bonferroni-corrected p-value <0.05 were considered to be significantly enriched within the lists of genes. GO categories enriched less than 2 out of the 44 groups were discarded. Fold enrichment of 27 significantly enriched GO slims was shown in heatmap.

Materials availability

All unique reagents generated in this study are available from the Lead Contact without restriction.

Data availability

Single cell data of recovery time and cell size and the RNA-seq data of gene expression FPKM value generated during this study are provided as datasheet. The original sequence data is available in NCBI BioProject database with the ID number of PRJNA900375. This study did not generate any unique code.

CRediT authorship contribution statement

Qi Liu: Writing – original draft, Visualization, Validation, Methodology, Investigation, Formal analysis, Data curation, Conceptualization. **Nan Sheng:** Writing – original draft, Visualization, Software, Methodology, Investigation, Formal analysis. **Zhiwen Zhang:** Visualization, Formal analysis. **Chenjun He:** Formal analysis. **Yao Zhao:** Formal analysis. **Haoyuan Sun:** Formal analysis. **Jianguo Chen:** Supervision. **Xiaojing Yang:** Writing – review & editing, Writing – original draft, Visualization, Validation, Supervision, Investigation, Funding acquisition, Formal analysis. **Chao Tang:** Writing – review & editing, Supervision, Investigation, Funding acquisition, Conceptualization.

Declaration of competing interest

The authors declare that they have no known competing financial interests or personal relationships that could have appeared to influence the work reported in this paper.

Acknowledgments

Appendix A. Supplementary data

Supplementary data to this article can be found online at https://doi.org/10.1016/j.heliyon.2024.e26558.

References

[1] T.H. Cheung, T.A. Rando, Molecular regulation of stem cell quiescence, Nat. Rev. Mol. Cell Biol. 14 (2013) 329–340.
[2] E.S.C. Rittershaus, S.H. Baek, C.M. Sassetti, The normalcy of dormancy: common themes in microbial quiescence, Cell Host Microbe 13 (2013) 643–651.
[3] A.S. Kaprelyants, J.C. Gottschal, D.B. Kell, Dormancy in non-sporulating bacteria, FEMS Microbiol. Lett. 104 (1993) 271–286.
[4] M. Rumman, J. Dhawan, M. Kassem, Concise review: quiescence in adult stem cells: biological significance and relevance to tissue regeneration, Stem Cell. 33 (2015) 2903–2912.
[5] Mathilde Latil, et al., Skeletal muscle stem cells adopt a dormant cell state post mortem and retain regenerative capacity, Nat. Commun. 3 (1) (2012) 903.
[6] S. Penfield, Seed dormancy and germination, Curr. Biol. 27 (2017) R874–R878.
[7] J. Heyman, R.P. Kumpf, L. De Veylder, A quiescent path to plant longevity, Trends Cell Biol. 24 (2014) 443–448.
[8] M. Gengenbacher, S.H.E. Kaufmann, Mycobacterium tuberculosis: success through dormancy, FEMS Microbiol. Rev. 36 (2012) 514–532.
[9] T.G. Phan, P.I. Croucher, The dormant cancer cell life cycle, Nat. Rev. Cancer 20 (2020) 398–411.
[10] V.D. Longo, G.S. Shadel, M. Kaeberlein, B. Kennedy, Replicative and chronological ageing in Saccharomyces cerevisiae, Cell Metabol. 16 (2012) 18–31.
[11] P. Fabrizio, V.D. Longo, The chronological life span of Saccharomyces cerevisiae, Aging Cell 2 (2) (2003) 73–81.
[12] V.D. Longo, E.B. Gralla, J.S. Valentine, Superoxide dismutase activity is essential for stationary phase survival in Saccharomyces cerevisiae - mitochondrial production of toxic oxygen species in vivo, J. Biol. Chem. 271 (1996) 12275–12280.
[13] P. Fabrizio, F. Pozza, S.D. Pletcher, C.M. Gendron, V.D. Longo, Regulation of longevity and stress resistance by Sch9 in yeast, Science 292 (2001) 288–290.
[14] D.L. Smith Jr., J.M. McClure, M. Matecic, J.S. Smith, Calorie restriction extends the chronological lifespan of Saccharomyces cerevisiae independently of the Sirtuins, Ageing Cell 6 (2007) 649–662.
[15] R.W. Powers, M. Kaeberlein, S.D. Caldwell, B.K. Kennedy, S. Fields, Extension of chronological life span in yeast by decreased TOR pathway signaling, Gene Dev. 20 (2006) 174–184.
[16] I. Orlandi, R. Ronzulli, N. Casatta, M. Vai, Ethanol and acetate acting as carbon/energy sources negatively affect yeast chronological ageing, 2013, Oxid. Med. Cell. Longev. (2013) 802870.
[17] Xinhe Huang, et al., Reducing signs of aging and increasing lifespan by drug synergy, Aging Cell 12 (4) (2013) 652–660.
[18] S.S. Su, Y. Tanaka, I. Samejima, K. Tanaka, M. Yanagida, A nitrogen starvation-induced dormant G0 state in fission yeast: the establishment from uncommitted G1 state and its delay for return to proliferation, J. Cell Sci. 109 (1996) 1347–1357.
[19] Kojiro Takeda, et al., Synergistic roles of the proteasome and autophagy for mitochondrial maintenance and chronological lifespan in fission yeast, Proc. Natl. Acad. Sci. USA 107 (8) (2010) 3540–3545.

[20] T. Sideri, C. Rallis, D.A. Bitton, B.M. Lages, F. Suo, M. Rodríguez-López, J. Bähler, Parallel profiling of fission yeast deletion mutants for proliferation and for lifespan during long-term quiescence, G3: Genes, Genomes, Genetics 5 (1) (2015) 145–155.

[21] C.A. Romila, S. Townsend, M. Malecki, S. Kamrad, M. Rodríguez-López, O. Hillson, J. Bähler, Barcode sequencing and a high-throughput assay for chronological lifespan uncover ageing-associated genes in fission yeast, Microbial Cell 8 (7) (2021) 146.

[22] A.E. Roux, A. Leroux, M.A. Alaamery, C.S. Hoffman, P. Chartrand, G. Ferbeyre, L.A. Rokeach, Pro-aging effects of glucose signaling through a G protein-coupled glucose receptor in fission yeast, PLoS Genet. 5 (3) (2009 Mar) e1000408.

[23] A.E. Roux, A. Quissac, P. Chartrand, G. Ferbeyre, L.A. Rokeach, Regulation of chronological ageing in Schizosaccharomyces pombe by the protein kinases Pka1 and Sck2, Ageing Cell 5 (2006) 345–357.

[24] L. Maestroni, J. Audry, S. Matmati, B. Arcangioli, V. Géli, S. Coulon, Eroded telomeres are rearranged in quiescent fission yeast cells through duplications of subtelomeric sequences, Nat. Commun. 8 (1) (2017) 1–14.

[25] Xinhe Huang, Markos Leggas, Robert C. Dickson, Drug synergy drives conserved pathways to increase fission yeast lifespan, PLoS One 10 (3) (2015) e0121877.

[26] Charalampos Rallis, et al., Systematic screen for mutants resistant to TORC1 inhibition in fission yeast reveals genes involved in cellular ageing and growth, Biology open 3 (2) (2014) 161–171.

[27] Bo-Ruei Chen, Kurt W. Runge, A new Schizosaccharomyces pombe chronological lifespan assay reveals that caloric restriction promotes efficient cell cycle exit and extends longevity, Exp. Gerontol. 44 (8) (2009) 493–502.

[28] D. Laporte, L. Jimenez, L. Gouleme, I. Sagot, Yeast quiescence exit swiftness is influenced by cell volume and chronological age, Microb Cell 5 (2018) 104–111.

[29] D. Laporte, A. Lebaudy, A. Sahin, B. Pinson, J. Ceschin, B. Daignan-Fornier, I. Sagot, Metabolic status rather than cell cycle signals control quiescence entry and exit, JCB (J. Cell Biol.) 192 (6) (2011) 949–957.

[30] Kenichi Sajiki, et al., Genetic control of cellular quiescence in S. pombe, J. Cell Sci. 122 (9) (2009) 1418–1429.

[31] I. Sagot, D. Laporte, The cell biology of quiescent yeast - a diversity of individual scenarios, J. Cell Sci. 132 (2019) jcs213025.

[32] M. Yanagida, Cellular quiescence: are controlling genes conserved? Trends Cell Biol. 19 (2009) 705–715.

[33] J.V. Gray, et al., "Sleeping beauty": quiescence in Saccharomyces cerevisiae, Microbiol. Mol. Biol. Rev. 68 (2004) 187–206.

[34] De Virgilio, Claudio, The essence of yeast quiescence, FEMS Microbiol. Rev. 36 (2) (2012) 306–339.

[35] I.J. Cho, P.P. Lui, J. Obajdin, F. Riccio, W. Stroukov, T.L. Willis, F.M. Watt, Mechanisms, hallmarks, and implications of stem cell quiescence, Stem Cell Rep. 12 (6) (2019) 1190–1200.

[36] H.A. Coller, The essence of quiescence, Science 334 (6059) (2011) 1074–1075.

[37] I. Sagot, D. Laporte, Quiescence, an individual journey, Curr. Genet. 65 (2019) 695–699.

[38] S. Marguerat, et al., Quantitative analysis of fission yeast transcriptomes and proteomes in proliferating and quiescent cells, Cell 151 (2012) 671–683.

[39] W. Wei, P. Nurse, D. Broek, Yeast cells can enter a quiescent state through G1, S, G2, or M phase of the cell cycle, Cancer Res. 53 (8) (1993) 1867–1870.

[40] M.M. Klosinska, C.A. Crutchfield, P.H. Bradley, J.D. Rabinowitz, J.R. Broach, Yeast cells can access distinct quiescent states, Genes & development 25 (4) (2011) 336–349.

[41] H.A. Coller, L. Sang, J.M. Roberts, A new description of cellular quiescence, PLoS Biol. 4 (3) (2006) e83.

[42] H. Baisch, Different quiescence states of three culture cell lines detected by acridine orange staining of cellular RNA, Cytometry: The Journal of the International Society for Analytical Cytology 9 (4) (1988) 325–331.

[43] P. Rocheteau, M. Vinet, F. Chretien, Dormancy and quiescence of skeletal muscle stem cells, Results Probl. Cell Differ. 56 (2015) 215–235.

[44] C. Allen, et al., Isolation of quiescent and nonquiescent cells from yeast stationary-phase cultures, J. Cell Biol. 174 (2006) 89–100.

[45] Anthony D. Aragon, et al., Characterization of differentiated quiescent and nonquiescent cells in yeast stationary-phase cultures, Mol. Biol. Cell 19 (3) (2008) 1271–1280.

[46] E. Herker, et al., Chronological ageing leads to apoptosis in yeast, J. Cell Biol. 164 (2004) 501–507.

[47] Charles S. Hoffman, Valerie Wood, Peter A. Fantes, An ancient yeast for young geneticists: a primer on the Schizosaccharomyces pombe model system, Genetics 201 (2) (2015) 403–423.

[48] V. Wood, et al., The genome sequence of Schizosaccharomyces pombe, Nature 415 (6874) (2002) 871–880.

[49] Satoru Mochida, Mitsuhiro Yanagida, Distinct modes of DNA damage response in S. pombe G0 and vegetative cells, Gene Cell. 11 (1) (2006) 13–27.

[50] M. Shimanuki, et al., Two-step, extensive alterations in the transcriptome from G0 arrest to cell division in Schizosaccharomyces pombe, Gene Cell. 12 (2007) 677–692.

[51] Takahiro Nakamura, et al., Impaired coenzyme A synthesis in fission yeast causes defective mitosis, quiescence-exit failure, histone hypoacetylation and fragile DNA, Open biology 2 (9) (2012) 120117.

[52] C. Gal, et al., The longevity and reversibility of quiescence in Schizosaccharomyces pombe are dependent upon the HIRA histone chaperone, Cell Cycle 22 (17) (2023) 1921–1936.

[53] Antoine E. Roux, et al., Fission yeast and other yeasts as emergent models to unravel cellular aging in eukaryotes, Journals of Gerontology Series A: Biomedical Sciences and Medical Sciences 65 (1) (2010) 1–8.

[54] A. Franco, et al., Quorum sensing: a major regulator of fungal development, in: T.G. Villa, T. de Miguel Bouzas (Eds.), Developmental Biology in Prokaryotes and Lower Eukaryotes, Springer, Cham, 2021.

[55] X.J. Yang, K.Y. Lau, V. Sevim, C. Tang, Design principles of the yeast G1/S switch, PLoS Biol. 11 (2013) e1001673.

[56] Benedikt Westermann, Bioenergetic role of mitochondrial fusion and fission, Biochim. Biophys. Acta Bioenerg. 1817 (10) (2012) 1833–1838.

[57] W. Li, H. Jiang, Nuclear protein condensates and their properties in regulation of gene expression, J. Mol. Biol. 434 (1) (2022) 167151.

[58] S.C. Li, P.M. Kane, The yeast lysosome-like vacuole: endpoint and crossroads, Biochim. Biophys. Acta 1793 (2009) 650–663.

[59] A. Nakashima, et al., A starvation-specific serine protease gene, isp6+, is involved in both autophagy and sexual development in Schizosaccharomyces pombe, Curr. Genet. 49 (2006) 403–413.

[60] T.A. Kohda, et al., Fission yeast autophagy induced by nitrogen starvation generates a nitrogen source that drives adaptation processes, Gene Cell. 12 (2007) 155–170.

[61] H. Mukaiyama, M. Nakase, T. Nakamura, Y. Kakinuma, K. Takegawa, Autophagy in the fission yeast Schizosaccharomyces pombe, FEBS Lett. 584 (2010) 1327–1334.

[62] N. Mizushima, M. Komatsu, Autophagy: renovation of cells and tissues, Cell 147 (2011) 728–741.

[63] J.A. Olzmann, P. Carvalho, Dynamics and functions of lipid droplets, Nat. Rev. Mol. Cell Biol. 20 (2019) 137–155.

[64] Q. Zhang, et al., Schizosaccharomyces pombe cells deficient in triacylglycerols synthesis undergo apoptosis upon entry into the stationary phase, J. Biol. Chem. 278 (2003) 47145–47155.

[65] A. Meyers, et al., Lipid droplets form from distinct regions of the cell in the fission yeast Schizosaccharomyces pombe, Traffic 17 (2016) 657–669.

[66] D.L. Fisher, P. Nurse, A single fission yeast mitotic cyclin B p34cdc2 kinase promotes both S-phase and mitosis in the absence of G1 cyclins, EMBO J. 15 (1996) 850–860.

[67] P. Gutierrez-Escribano, P. Nurse, A single cyclin-CDK complex is sufficient for both mitotic and meiotic progression in fission yeast, Nat. Commun. 6 (2015) 1–13.

[68] I. Hagan, J. Hayles, P. Nurse, Cloning and sequencing of the cyclin-related Cdc13+ gene and a cytological study of its role in fission yeast mitosis, J. Cell Sci. 91 (1988) 587–595.

[69] S. Moreno, P. Nurse, Regulation of progression through the G1 phase of the cell-cycle by the Rum1(+) gene, Nature 367 (1994) 236–242.

[70] R.R. Daga, P. Bolanos, S. Moreno, Regulated mRNA stability of the Cdk inhibitor Rum1 links nutrient status to cell cycle progression, Curr. Biol. 13 (2003) 2015–2024.

[71] Damien Laporte, et al., Reversible cytoplasmic localization of the proteasome in quiescent yeast cells, J. Cell Biol. 181 (5) (2008) 737–745.

[72] Kenrick A. Waite, et al., Starvation induces proteasome autophagy with different pathways for core and regulatory particles, J. Biol. Chem. 291 (7) (2016) 3239–3253.

[73] R. Weisman, Fission yeast TOR and rapamycin, in: The Enzymes (Vol. 27, Pp. 251-269), Academic Press, 2010.

[74] L.E. Backhus, et al., Functional genomic analysis of a commercial wine strain of Saccharomyces cerevisiae under differing nitrogen conditions, FEMS Yeast Res. 1 (2) (2001) 111–125.

[75] S.L. Forsburg, N. Rhind, Basic methods for fission yeast, Yeast 23 (2006) 173–183.

[76] M.D. Krawchuk, W.P. Wahls, High-efficiency gene targeting in Schizosaccharomyces pombe using a modular, PCR-based approach with long tracts of flanking homology, Yeast 15 (1999) 1419–1427.

[77] J. Schindelin, et al., Fiji: an open-source platform for biological-image analysis, Nat. Methods 9 (2012) 676–682.

[78] Y.X. Chen, et al., SOAPnuke: a MapReduce acceleration-supported software for integrated quality control and preprocessing of high-throughput sequencing data, GigaScience 7 (2017) gix120.

[79] D. Kim, J.M. Paggi, C. Park, C. Bennett, S.L. Salzberg, Graph-based genome alignment and genotyping with HISAT2 and HISAT-genotype, Nat. Biotechnol. 37 (2019) 907–915.

[80] B. Langmead, S.L. Salzberg, Fast gapped-read alignment with Bowtie 2, Nat. Methods 9 (2012) 357–359.

[81] B. Li, C.N. Dewey, RSEM: accurate transcript quantification from RNA-Seq data with or without a reference genome, BMC Bioinf. 12 (2011) 1–16.

[82] P. Langfelder, S. Horvath, WGCNA: an R package for weighted correlation network analysis, BMC Bioinf. 9 (2008) 1–13.

[83] G.C. Yu, L.G. Wang, Y.Y. Han, Q.Y. He, clusterProfiler: an R Package for comparing biological themes among gene clusters, OMICS 16 (2012) 284–287.

[84] M.I. Love, W. Huber, S. Anders, Moderated estimation of fold change and dispersion for RNA-seq data with DESeq2, Genome Biol. 15 (2014) 1–21.